Published online 21 November 2012 *Nucleic Acids Research, 2013, Vol. 41, No. 2* ***1029–1046***
doi:10.1093/nar/gks1088

Physical and functional interaction between yeast Pif1 helicase and Rim1 single-stranded DNA binding protein

Ramanagouda Ramanagoudr-Bhojappa, Lauren P. Blair, Alan J. Tackett and Kevin D. Raney*

Department of Biochemistry and Molecular Biology, University of Arkansas for Medical Sciences, Little Rock, AR 72205-7199, USA

Received August 7, 2012; Revised October 15, 2012; Accepted October 17, 2012

ABSTRACT

Pif1 helicase plays various roles in the maintenance of nuclear and mitochondrial genome integrity in most eukaryotes. Here, we used a proteomics approach called isotopic differentiation of interactions as random or targeted to identify specific protein complexes of *Saccharomyces cerevisiae* Pif1. We identified a stable association between Pif1 and a mitochondrial SSB, Rim1. *In vitro* co-precipitation experiments using recombinant proteins indicated a direct interaction between Pif1 and Rim1. Fluorescently labeled Rim1 was titrated with Pif1 resulting in an increase in anisotropy and a K_d value of 0.69 μM. Deletion mutagenesis revealed that the OB-fold domain and the C-terminal tail of Rim1 are both involved in interaction with Pif1. However, a Rim1 C-terminal truncation (Rim1ΔC18) exhibited a nearly 4-fold higher K_d value. Rim1 stimulated Pif1 DNA helicase activity by 4- to 5-fold, whereas Rim1ΔC18 stimulated Pif1 by 2-fold. Hence, two regions of Rim1, the OB-fold domain and the C-terminal domain, interact with Pif1. One of these interactions occurs through the N-terminal domain of Pif1 because a deletion mutant of Pif1 (Pif1ΔN) retained interaction with Rim1 but did not exhibit stimulation of helicase activity. In light of our *in vivo* and *in vitro* data, and previous work, it is likely that the Rim1–Pif1 interaction plays a role in coordination of their functions in mtDNA metabolism.

INTRODUCTION

Helicases are nucleic acid stimulated motor enzymes that catalyze the unwinding of duplex nucleic acids using ATP as their energy source. They play a vital role in DNA metabolism and help to conserve genome integrity. The Pif1 family of helicases has been identified in most eukaryotes and is involved in the maintenance of both nuclear and mitochondrial genomes (1). Pif1 from *Saccharomyces cerevisiae* is the prototypical helicase from the Pif1 family. It has homologs in a wide range of species, such as *Homo sapiens*, *Mus musculus, Drosophila melanogaster* and *Caenorhabditis elegans*, including its budding yeast homolog Rrm3 and fission yeast homolog Pfh1 (1,2). Although Pif1 is transcribed from a single open reading frame, it has two in-frame translation start codons which regulate the localization of the protein to either the mitochondria or the nucleus (3).

Pif1 was discovered in a forward genetics study that selected genes affecting the recombination of mitochondrial DNA (mtDNA) in yeast (4,5). The high-frequency recombination between the rho^+ and rho^- mitochondrial genomes is affected in the absence of Pif1 (4). Pif1 is also involved in maintenance of mtDNA (5–7), and repair of damage induced by reactive oxygen species (8). In addition, genotoxic chemicals such as ethidium bromide increase sensitivity and region-specific mtDNA breakage in the absence of Pif1, suggesting that Pif1 either prevents or helps to repair dsDNA breaks in mtDNA (7,9).

In the nucleus, Pif1 localizes to specific chromosomal loci and participates in multiple biological functions. Pif1 negatively regulates telomere lengths by catalytically inhibiting telomerase activity (3,10). Repair of DNA is facilitated by Pif1-mediated removal of telomerase at dsDNA breaks (11,12). Other functions affected by Pif1 activity are Okazaki fragment maturation (13,14), ribosomal DNA replication (15) and processing of G-quadruplex structures (16).

Pif1 belongs to the SF1B family of helicases and unwinds DNA with 5′→3′ polarity in an ATP dependent manner (17,18). It reportedly exists as monomer in

*To whom correspondence should be addressed. Tel: +1 501 686 5244; Fax: +1 501 686 8169; Email: raneykevind@uams.edu
Present address:
Lauren P. Blair, Department of Pathology, Yale University School of Medicine, New Haven, CT 06510, USA.

solution (17), but dimerizes upon binding to ssDNA (19). Pif1 unwinds shorter duplexes more efficiently than longer duplexes, suggesting that it has relatively low processivity (17). DNA:RNA heteroduplexes and G-quadruplex substrates are favored by Pif1 compared with DNA:DNA substrates (16,20). A recent report on Pif1 telomere regulation shows that phosphorylation at the C-terminus is required for inhibition of *de novo* telomere addition at dsDNA breaks but not for inhibiting the addition of telomere repeats at telomere ends (21).

Despite the range of functions, the protein interaction networks that likely modulate Pif1 activity are not well-characterized. Similar to Pif1, the helicases of the RecQ family are known to have multiple biological functions associated with the maintenance of genome integrity. RecQ family helicases from both eukaryotes and prokaryotes have extensive protein interaction networks of functional significance (22,23). A physical interaction between RecQ homologs and topoisomerase III has been identified in both yeast and human cells, and these interactions are essential for the proper functioning of RecQ helicases (24). RecQ5 interaction with Rad51 is proposed to play a critical role in anti-recombinase activity (25). *Escherichia coli* RecQ was found to interact with SSB, ExoI and RecJ all of which have functional significance (22,26).

The eukaryotic SSB proteins, RPA and POT1 are known to specifically stimulate WRN helicase activity *in vitro* (27). The functional interaction between WRN and RPA has been proposed to assist in resolution of replication fork blocks (28). *Escherichia coli* PriA helicase interacts with *Ec*SSB protein to coordinate replication fork reloading (29), and to mediate interaction with PriB to form the PriA–PriB complex (30). Human mitochondrial SSB (*Hs*mtSSB) has been shown to interact physically and functionally with the human mtDNA helicase (Twinkle helicase) (31). Mutations in Twinkle helicase are known to cause progressive external ophthalmoplegia, a condition associated with multiple deletions in the mtDNA (32). At the mtDNA replication fork, *Hs*mtSSB interacts functionally with Twinkle helicase and DNA polymerase γ (pol γ) to promote mtDNA replication (33,34).

Identification of protein–protein interactions has been facilitated by use of the tandem affinity purification (TAP) technique followed by mass spectrometry (35,36). However, this technique is often compromised by co-enrichment of nonspecific interactors or false positives. To overcome this problem, a mass spectrometric strategy has been developed called isotopic differentiation of interactions as random or targeted (I-DIRT) (37). In this study, we conducted a proteomic investigation using I-DIRT to identify Pif1 interacting partners that may help decipher some of the mechanisms by which Pif1 is regulated. We identified a stable and specific interaction between Pif1 and the mitochondrial SSB, Rim1. Interestingly, Rim1 was discovered as a suppressor of a thermosensitive phenotype of a *pif1* null mutant, indicating a genetic interaction between these two proteins (6). We demonstrate a direct physical interaction between these proteins regulated by two binding regions on each of the proteins. Rim1 stimulates the helicase activity of Pif1 on DNA substrates that favor binding of Rim1.

MATERIALS AND METHODS

Reagents

4-(2-hydroxyethyl)-1-piperazineethanesulfonic acid (HEPES), Tris, NaCl, ethylenediaminetetraacetic acid (EDTA), bovine serum albumin (BSA), $MgCl_2$, sodium dodecyl sulphate (SDS), KOH, β-mercaptoethanol (BME), acrylamide, bisacrylamide, formamide, xylene cyanol, bromophenol blue, urea and glycerol were purchased from Fisher Scientific. Phosphoenolpyruvate (PEP) (tricyclohexylammonium salt), pyruvate kinase/lactate dehydrogenase (in glycerol), ATP (disodium salt), poly(dT), NADH and Sephadex G-25 were obtained from Sigma. [γ-^{32}P]ATP was obtained from Perkin-Elmer Life Sciences. All the DNA oligonucleotides were obtained from Integrated DNA Technologies, purified using denaturing polyacrylamide gel electrophoresis, and quantified by UV absorbance at 260 nm. T4 polynucleotide kinase and all restriction enzymes were obtained from New England Biolabs. Epoxy-270 Dynabeads, 4–20% NuPAGE gels and 5-carboxyfluorescein succinimidyl ester (5-FAM SE) were purchased from Invitrogen. DL-Lysine-4,4,5,5-d4 2HCl was purchased from C/D/N Isotopes Inc. GelCode Blue was from Pierce Chemical. Coomassie Plus Protein assay reagent was from Thermo Scientific.

Yeast strains and growth conditions

Saccharomyces cerevisiae BY4741 parent strain and PIF1::TAP-HIS3 BY4741 strain (C-terminal TAP-tag) were used for all protocols under growth conditions as described (37). The PIF1-TAP tagged strain was grown till mid-log phase in a synthetic complete medium (light isotopic medium), whereas the parent strain was grown till mid-log phase in a synthetic complete medium where h4-lysine was substituted by DL-lysine-4,4,5,5-d4 2HCl. The cultured cells were harvested by centrifugation and frozen as pellets using liquid nitrogen. Equal amounts of isotopically light and heavy cell pellets were mixed and disrupted with a Retsch MM301 mixer mill maintained with liquid nitrogen and stored at −80°C (37).

Immunoisolation and I-DIRT

Affinity purification of Pif1-TAP and its associated proteins was performed using IgG-coated Epoxy-270 Dynabeads at 300 mM NaCl (37). Briefly, 10 g of disrupted cell mixture was resuspended in 50 ml immunopurification (IP) buffer (20 mM HEPES pH 7.4, 300 mM NaCl, 2 mM $MgCl_2$, 1 mg DNase I, 0.1% Tween-20, 1/100 protease inhibitor cocktail), incubated with 40 mg of IgG-coated Dynabeads and rotated for 2 h at 4°C. Dynabeads were captured with a magnet and washed five times with IP buffer to reduce nonspecific interactors. Captured Dynabeads were treated with 0.5 M ammonium hydroxide to elute associated protein complexes. Immunoisolated protein complexes were resolved on a

4–20% NuPAGE gel and visualized by Coomassie staining with GelCode Blue. The entire gel lane was sliced into 38 equal sections, subjected to tryptic digestion and peptides were analyzed by matrix-assisted laser desorption/ionization mass spectrometry (MALDI-MS). High resolution spectra of peptides were collected with a PerkinElmerSciex MALDI-prOTOF mass spectrometer, while tandem mass spectra were collected with a Thermo vMALDI-LTQ mass spectrometer. Tandem mass spectrometry data were analyzed using XProteo software. Peptides containing either one or two lysine residues were visualized using M-over-Z software. The appearance of isotopically heavy versions of each peptide was recorded with a 4 or 8 Da higher mass depending on the presence of one or two d4-lysines, respectively. The fraction area under light peptides was calculated as described (37).

Generation of recombinant proteins

The open reading frame coding for the mature Rim1 protein (excluding the Mitochondrial Targeting Signal) was cloned into the pSUMO vector with an N-terminal SUMO-tag. The fusion protein was overexpressed in Rosetta 2 (DE3) cells with 0.5 mM isopropyl β-D-1-thiogalactopyranoside (IPTG) induction and purified as described (38) with minor modifications. Briefly, the cell pellet was suspended in buffer (50 mM sodium phosphate buffer pH 7.5, 300 mM NaCl, 5 mM BME and 10% glycerol) with 0.5 mg/ml lysozyme and passed through a microfluidizer to lyse the cells. The lysate was subjected to ultracentrifugation at 100 000*g* for 1 h. The supernatant was applied onto a TALON metal affinity resin (Clontech) and washed with five bed volumes of buffer containing 20 mM imidazole. Proteins bound to the column were eluted using buffer containing 200 mM imidazole. SUMO-Rim1 fusion protein was subjected to Ulp1 protease cleavage to separate the N-terminal SUMO-tag (with His-tag) from the Rim1 protein. The protease cleaved sample was applied to fresh TALON metal affinity resin to trap the SUMO-tag, Ulp1 protease (with His-tag) and remaining contaminants from the first Talon column, whereas the native Rim1 protein without any tags eluted in the flow-through fraction. Rim1 protein was further purified by passing it through a strong anion exchange column (Macro-Prep High Q Support, Bio-Rad) with a gradient salt elution of 150 mM to 2 M NaCl. The fractions containing pure Rim1 protein were pooled and concentrated using centrifugal filter units (Millipore) and stored at −80°C in storage buffer (25 mM HEPES pH 7.5, 150 mM NaCl, 2 mM BME, 0.1 mM EDTA and 30% glycerol). Protein concentrations were determined by UV absorbance and Coomassie Plus Protein assay using BSA as a standard. A Rim1 variant with a deletion of 18 amino acids from the C-terminal end (Rim1ΔC18) was created using site-directed mutagenesis. The plasmid for *Hs*mtSSB protein in the pSUMO vector was a gift from Craig Cameron. Rim1ΔC18 and *Hs*mtSSB proteins were overexpressed and purified similarly to Rim1. The protein concentrations of Rim1, Rim1ΔC18 and *Hs*mtSSB were calculated in tetramers. The detailed protocol for the cloning, expression and purification of Pif1 protein and its characterization is described in the Supplementary Materials and Methods.

Size-exclusion chromatography with multi-angle light scattering

Size-exclusion chromatography with multi-angle light scattering (SEC-MALS) experiments were performed for Rim1 (260 μg) and Rim1ΔC18 (70 μg) protein samples as described (39). Briefly, the SEC column for multi-angle scattering (WTC-030S5, Wyatt Technology) was equilibrated with a buffer containing 50 mM HEPES pH 7.5, 0.1 M NaCl, 0.1 M KCl, 1 mM tris(2-carboxyethyl)-phosphine, 5 mM BME and 1% glycerol at a flow rate of 0.5 ml/min using a Shimadzu HPLC instrument. Protein eluting from the column was analyzed by three detectors placed in series in the following order: a UV detector (A280, Shimadzu), a DAWN HELEOS-II 18-angle light scattering detector (LS, Wyatt Technology) and an Optilab T-rEX Differential Refractometer (dRI, Wyatt Technology). The differential index of refraction (d*n*/d*c*) value of 0.185 ml/mg was used for the analysis. Protein sample in the buffer (100 μl) was loaded on to the SEC column at a flow rate of 0.5 ml/min. The protein molecular mass (MM) and hydrodynamic radius (R_h) were calculated from the light scattering data using Astra 6 software.

DNA binding fluorescence anisotropy assay

Anisotropy of fluorescein labeled ssDNA was measured to determine the binding affinity of SSB proteins at 25°C in buffer (25 mM HEPES pH 7.5, 50 mM NaCl, 10 mM $MgCl_2$, 0.1 mM EDTA, 2 mM BME and 0.1 mg/ml BSA) as described (40). A solution containing 1 nM of 3′-fluorescein T_{20} (3′F-T_{20}) or 3′-fluorescein T_{70} (3′F-T_{70}) was incubated with increasing concentrations of SSB protein. Fluorescence polarization values were measured using a PerkinElmer Life Sciences Victor^{3}V 1420 with excitation and emission wavelengths set to 485 and 535 nm, respectively. Fluorescence anisotropy was calculated and plotted versus concentration of SSB using KaleidaGraph. The data for 3′F-T_{20} were fit to the Hill equation to obtain a Hill coefficient and apparent K_d value.

Co-precipitation by protein coated Dynabeads

Purified recombinant SSB proteins (Rim1, Rim1ΔC18 and *Hs*mtSSB), BSA and glycine were covalently cross-linked onto epoxy-activated Dynabeads M-270 (Invitrogen) as per the manufacturer's instructions. Saturating amounts of protein were used for coating 2.5 mg of epoxy-activated Dynabeads at 37°C for 24 h. Co-precipitation experiments were performed by incubating purified Pif1 protein (20 μg) with SSB-coated beads in a buffer containing 25 mM HEPES pH 7.5, 250 mM NaCl, 2 mM $MgCl_2$, 2 mM BME, 0.1 mM EDTA, 0.1 mg/ml BSA, 0.1% Tween-20 and 5% glycerol. SSB-coated beads and Pif1 were incubated together in a 300-μl buffer with rotation at 4°C for 2 h. Dynabeads were captured using a magnet and washed five times in 1 ml of buffer. Pif1 protein that co-precipitated

with the beads was eluted upon addition of 50 µl of Laemmli sample buffer and heating at 95°C for 5 min. The sample (20 µl) was resolved by 4–20% NuPAGE gel and the proteins were visualized by Coomassie staining with GelCode Blue.

Ammonium sulfate co-precipitation

Ammonium sulfate co-precipitation was performed as described (22) with minor modifications. Briefly, Pif1 (5 µM) was preincubated with SSB protein (5 µM) in a 20-µl reaction buffer containing 10 mM Tris pH 7.5, 150 mM NaCl and 10% glycerol on ice for 20 min. In total, 20 µl of saturated ammonium sulfate (~540 g/l) was added to the reaction and incubated on ice for an additional 30 min followed by centrifugation for 2 min at 13 000g. The supernatant (40 µl) was removed and resuspended in 10 µl of 4× Laemmli sample buffer. The pellet was washed twice with co-precipitation buffer containing 270 g/l ammonium sulfate then resuspended in 50 µl of 1× Laemmli loading buffer. Fifteen microliter of each sample was resolved on 15% Sodium dodecyl sulphate-polyacrylamide gel electrophoresis (SDS–PAGE) gel and stained using GelCode Blue.

Fluorescein dye labeling

Proteins (~2 mg/ml Rim1 or Rim1ΔC18) were prepared in a buffer containing 100 mM sodium bicarbonate pH 8.5, 200 mM NaCl and 0.1 mM EDTA. The fluorescein derivative, 5-FAM SE, was reconstituted in dimethyl sulfoxide at 1 mg/ml and added to the protein solution at a dye:protein molar ratio of ~3:1 (monomer). After mixing, the solution was incubated at room temperature for 1 h. Nonreacted dye was removed by gel filtration on a G-25 sephadex column. Protein concentration and the degree of labeling (DOL) were calculated according to the manufacturer's instructions. Protein labeled 5-FAM has an excitation of 498 nm and emission wavelength of 520 nm.

Protein binding fluorescence anisotropy assay

Experiments were conducted at 25°C in a buffer containing 25 mM HEPES pH 7.5, 100 mM NaCl, 0.1 mM EDTA, 2 mM BME and 0.1 mg/ml BSA. In a microtiter plate, a solution containing 5-FAM-labeled SSB (100 nM) was incubated with increasing concentrations of Pif1 or Pif1ΔN protein. Fluorescence polarization values were measured using a BioTek Synergy 4 hybrid multi-mode plate reader with band pass excitation and emission wavelength filters of 485/20 and 528/20 nm, respectively. Fluorescence anisotropy was calculated and plotted versus concentration of Pif1 or Pif1ΔN using KaleidaGraph. The data were fit to the equation for a hyperbola to obtain the dissociation constant (K_d) value.

Multiple turnover DNA unwinding

Two DNA substrates made up of partial duplexes, 70T30bp and 20T30bp (Table 1), were prepared and radiolabeled on the displaced strand (30mer) as described (41). All concentrations listed are after initiation of the DNA unwinding reaction. The unwinding experiments were performed at 25°C in a buffer containing 25 mM HEPES pH 7.5, 50 mM NaCl, 10 mM $MgCl_2$, 0.1 mM EDTA, 2 mM BME and 0.1 mg/ml BSA. Reactions contained 2 nM DNA substrate and 5 mM ATP and initiated upon the addition of 100 nM Pif1 and 60 nM unlabeled 30mer that served to trap the complementary loading strand after strand separation. Unwinding experiments in the presence of SSB proteins were performed by preincubating 100 nM SSB protein with a mixture containing 2 nM substrate and 5 mM ATP for 5 min before addition of 100 nM Pif1 and 60 nM unlabeled 30mer. At desired times, aliquots of the reaction mixture were transferred to the quench solution (200 mM EDTA, 0.6% SDS, 0.1% bromophenol blue, 0.1% xylene cyanol, 6% glycerol and 112 µM T_{70}). The role of the T_{70} in the quench solution was to sequester proteins after the reaction. The substrate and ssDNA product were resolved on a 20% native polyacrylamide gel. Radiolabeled substrate and product were detected using a Typhoon Trio PhosphorImager (GE Healthcare) and quantified using ImageQuant software. The amount of product formed over time was plotted using KaleidaGraph. The unwinding data were fit to a single exponential.

ATPase activity assay

The ATPase activity of purified Pif1 protein was measured at 25°C using a coupled spectrophotometric assay (42). The ATPase activity at increasing concentrations of poly(dT) was determined using 100 nM Pif1 in an ATPase assay buffer containing 25 mM HEPES (pH 7.5), 5 mM ATP, 10 mM $MgCl_2$, 50 mM NaCl, 0.1 mg/ml BSA, 1 mM BME, 4 mM PEP, 10 U/ml pyruvate kinase, 15 U/ml lactate dehydrogenase and 0.9 mM NADH. The ATP hydrolysis rates were determined by measuring the conversion of NADH to NAD^+ at 380 nm. The ATPase activity was plotted versus increasing concentration of poly(dT) using KaleidaGraph and data were fit to the equation for a hyperbola. In a separate experiment, ATPase activity of Pif1 (20 nM) was measured in the presence of increasing concentrations of Rim1 at a fixed concentration of poly(dT) (20 µM nt).

RESULTS

Pif1 and mitochondrial SSB Rim1 have a specific and stable interaction *in vivo*

TAP-tagged immunoisolation is a powerful technique for identifying stable protein complexes. However, association of nonspecific interactors with TAP-tagged complexes is one of the major problems associated with this method. We used a technique called I-DIRT, which helps to distinguish specific from nonspecific interactions (Figure 1A). In the I-DIRT technique, the yeast strain expressing Pif1-TAP is grown in light-isotopic media and the wild-type strain is grown in heavy-isotopic media. Mixing the cell lysates from each growth allows for discernment of specific from nonspecific interactors

Table 1. Partial duplex substrates used in unwinding experiments

Substrate	Strand	Length (nt)	Oligonucleotide sequence
70T30bp	LS	100	5′-$(T)_{70}$ CTG CTG CCA TGT CAC GCT GAT GTC GCC TGT-3′
	DS	30	3′-GAC GAC GGT ACA GTG CGA CTA CAG CGG ACA-5′
20T30bp	LS	50	5′-$(T)_{20}$ CTG CTG CCA TGT CAC GCT GAT GTC GCC TGT-3′
	DS	30	3′-GAC GAC GGT ACA GTG CGA CTA CAG CGG ACA-5′
14T16bp DNA:DNA	LS	30	5′-$(T)_{14}$ CGC TGA TGT CGC CTG G-3′
	DS	16	3′-GCG ACT ACA GCG GAC C-5′
14T20bp DNA:DNA	LS	34	5′-$(T)_{14}$ CGC TGA TGT CGC CTG GTA CG-3′
	DS	20	3′-GCG ACT ACA GCG GAC CAT GC-5′
14T16bp DNA:RNA	LS	30	5′-$(T)_{14}$ CGC TGA TGT CGC CTG T-3′
	DS (RNA)	16	3′-GCG ACU ACA GCG GAC A-5′

LS, loading strand; DS, displaced strand.

after immunoisolation of the TAP-tagged protein. The specifically associated proteins that are tightly bound to the Pif1-TAP complex *in vivo* contain only isotopically light proteins. We performed a Pif1-TAP pull-down experiment from a mixture of equal amounts of light and heavy cell lysate using IgG-coated Dynabeads for immunoisolation under stringent conditions (300 mM NaCl). Protein complexes that co-purified with Pif1-TAP were resolved on a SDS–PAGE gel and visualized by Coomassie blue staining (Figure 1B). Trypsin-derived peptides from the gel were identified using MALDI-prOTOF MS and vMALDI-LTQ MS^2. Apart from Pif1 itself, 23 proteins were identified (Supplementary Table S1). The M-over-Z program was used to visualize a single peptide mass spectrum of the h4-lysine-containing peptides and its corresponding d4-lysine-containing peptides. Presence of each d4-lysine will add 4 Da to the corresponding light-peptide. Figure 1C shows a representative mass spectrum of three distinct peptides from three different proteins identified from the experiment. The mass spectra of h4- and d4-lysine containing Ssb2 peptides have a mass-to-charge ratio (m/z) of 1394.8 and 1398.8 Da, respectively. Presence of equal amounts of both light and heavy peptides of Ssb2 protein illustrates its association with Pif1-TAP after cell lysis, hence Ssb2 is considered as a nonspecific interactor of Pif1. Only Rim1 peptides, apart from the expected Pif1 peptides, exhibited mass spectra for isotopically light peptides and no spectra for heavy peptides, indicating that Rim1 specifically interacts with Pif1.

The monoisotopic peak area under light and heavy peptides was calculated after subtracting background, and used to determine the fraction area for the light peptide. The fraction area under the light peptide for Pif1 and Rim1 is ~1, whereas the fraction area is ~0.6 for the remaining proteins identified (Figure 1D; Supplementary Table S1). The majority of the nonspecific proteins identified were either ribosomal or heat shock proteins, which are known common contaminants because of their abundance in the cell. A few of the proteins that were identified as nonspecific were nonribosomal and nonheat shock proteins including Tef2 (translation elongation factor), Tdh3 (triose-phosphate dehydrogenase), Mrm2 (mitochondrial rRNA methyl transferase) and H2A1 (Histone 2 A).

Purification and characterization of Pif1 protein

To investigate the functional significance of the interaction between Pif1 and Rim1, recombinant proteins were purified to homogeneity. Overexpression of the nuclear form of Pif1 under the T7 expression system in *E. coli* cells revealed an internal RBS site that dramatically reduced the total protein yield. A silent mutation was placed in the internal ribosomal binding site (RBS) site, followed by expression of Pif1 as a SUMO fusion which lead to improved protein expression and purification (Supplementary Figure S1A and B). Purification of Pif1 was followed by characterization of unwinding activity using substrates shown in Table 1. Strand-separation activity of Pif1 was comparable with published reports (Supplementary Figure S1D) (17,20).

Physicochemical characterization of Rim1 protein

Bacterial SSBs and eukaryotic mitochondrial SSBs show very high homology in the DNA binding domain (OB-fold domain) but show little or no homology in the C-terminal tail regions (43,44). Reported crystal structures for these SSBs have shown that the OB-fold domains are very similar, whereas the C-terminal tails exhibit a disordered structure (45–48). Some SSBs bind to multiple proteins by using the C-terminal tail as a docking site for the interaction. The C-terminal tail of *Ec*SSB has a stretch of conserved acidic residues, which facilitate interaction with multiple proteins (22,49). The sequence alignment of eukaryotic mtSSBs, bacterial SSBs and Rim1 is shown in Figure 2A. The OB-fold domain of Rim1 likely includes 100 amino acids from the N-terminal end, whereas the remaining 18 amino acids at the C-terminal end are predicted to form the tail region (Figure 2A). Acidic residues are observed at the C-terminus of Rim1, but they do not appear to correspond to the conserved acidic stretch at the C-terminal end of *Ec*SSB.

Rim1 and a C-terminal truncated form (Rim1ΔC18) were cloned, expressed and purified to homogeneity (Figure 2B). The bacterial SSBs and eukaryotic mitochondrial SSBs exist as homotetramers in solution (43,45,46). We examined the oligomeric nature of purified Rim1 and Rim1ΔC18 proteins using SEC-MALS. We used an 18-angle light scattering detector for the measurement of absolute molar mass and sizes of molecules without relying on calibration of standards. The theoretical

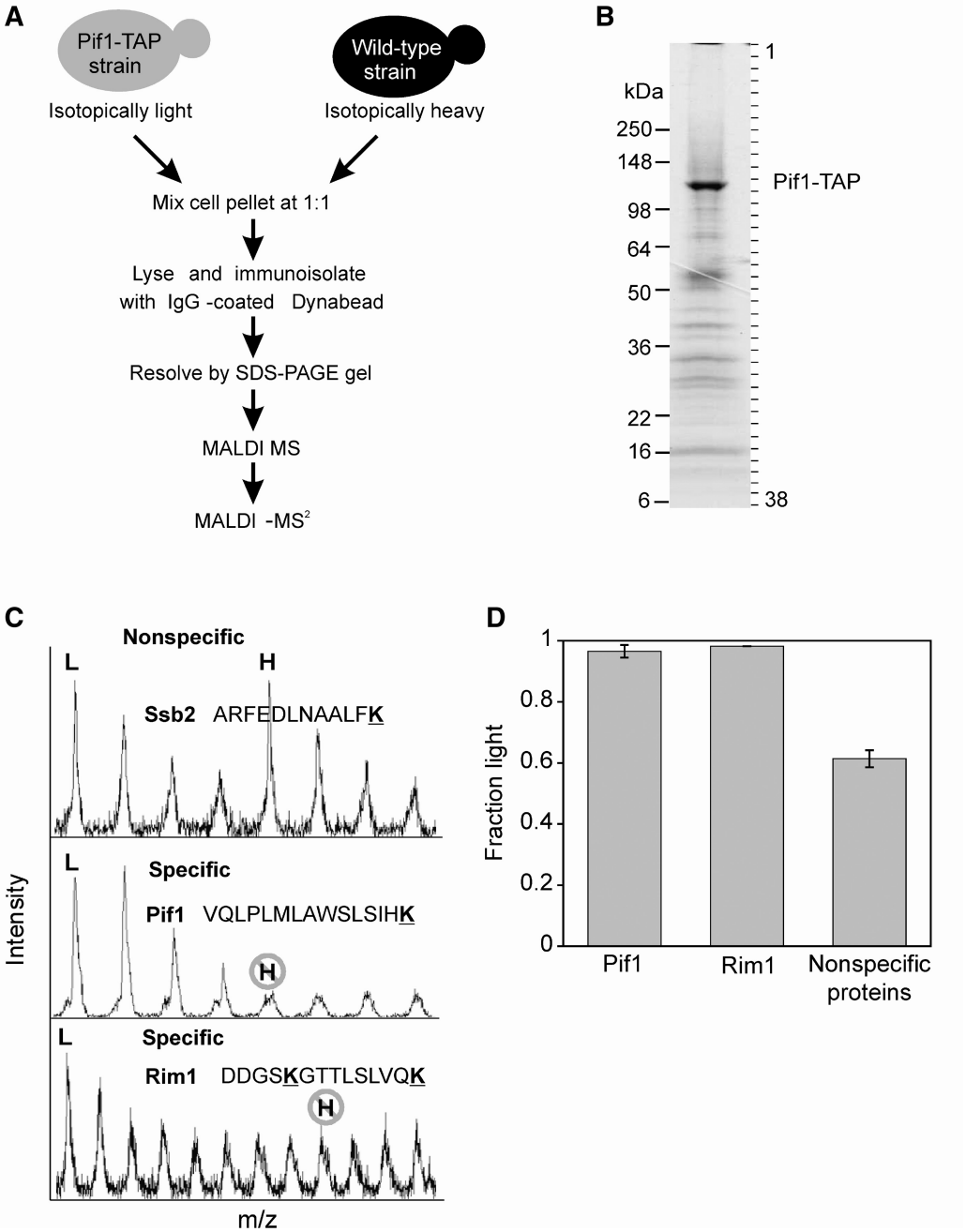

Figure 1. Identification of specific protein complexes of Pif1 in *S. cerevisiae* using I-DIRT. (**A**) Schematic representation of the I-DIRT procedure. Pif1-TAP tag strains were cultured in a light isotopic media, whereas the parent strains were cultured in heavy isotopic media containing d4-lysine. Equal quantities of cell lysates were mixed and subjected to affinity capture for the Pif1-TAP protein complex followed by SDS–PAGE and MS analysis. (**B**) Immunoisolated Pif1-TAP and its associated proteins were resolved by SDS–PAGE on a 4–20% NuPAGE gel and visualized by Coomassie blue staining. (**C**) Representative mass spectra of peptides from the Pif1 I-DIRT experiment. A peptide from the Ssb2 protein containing a single lysine exhibits both isotopically light (1394.8 Da) and heavy (1398.8 Da) peptides. The Rim1 peptide has two lysines with the monoisotopic peak exhibiting only isotopically light peptides (1448.76 Da). As expected, the peptides of Pif1 protein exhibited only the monoisotopic peak for isotopically light peptides. (**D**) For each of the lysine containing peptides identified by MS, the peak area under the isotopically light peptides was compared with the peak area for the heavy peptides to obtain a 'fraction light'. Twenty two proteins were identified as nonspecific interactors due to one or more peptides having a light to heavy ratio of ~0.6. In contrast, the fraction of light to heavy peptides for Rim1 and Pif1 proteins was ~1. All the identified proteins and their average 'fraction light' areas are listed in Supplementary Table S1.

molar mass of monomeric Rim1 and Rim1ΔC18 are 13.29 and 11.43 kDa, respectively. The molar mass determined by MALS analysis yielded 50 830 ± 0.3% Da for Rim1 and 44 730 ± 0.4% Da for Rim1ΔC18. These results indicate that both the proteins exist as tetramers in solution. We estimated the hydrodynamic radius (R_h) for Rim1 and Rim1ΔC18 using dynamic light scattering data. The R_h value for Rim1 was 3.3 ± 0.4% nm, whereas for Rim1ΔC18 was 2.0 ± 0.6% nm. The R_h value for Rim1ΔC18 protein is in correlation with the linear

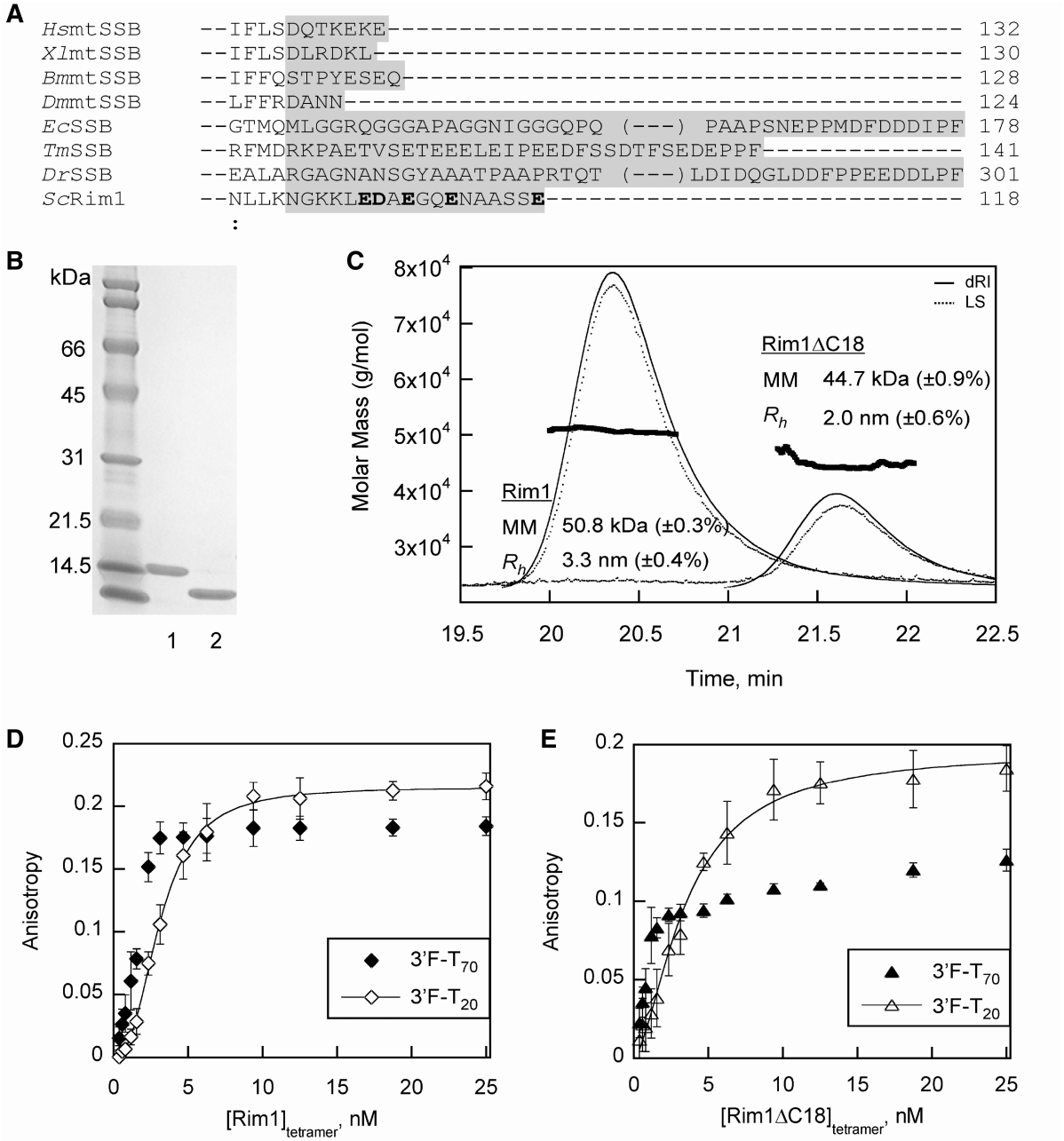

Figure 2. Purification and characterization of recombinant Rim1 protein and its C-terminal truncation variant. (**A**) Multiple sequence alignment of eukaryotic mitochondrial SSBs and bacterial SSBs using the ClustalW2 program to determine the C-terminal tail region of Rim1. The sequences for *H. sapiens* mtSSB (*Hs*mtSSB) (GenBank^{TM} accession: NP_003134), *Xenopus laevis* mtSSB (*Xl*mtSSB) (GenBank^{TM} accession: NP_001095241), *Bombyx mori* mtSSB (*Bm*mtSSB) (GenBank^{TM} accession: ABF51293), *D. melanogaster* mtSSB (*Dm*mtSSB) (GenBank^{TM} accession: AAF16936), *E. coli* SSB (*Ec*SSB) (GenBank^{TM} accession: YP_859663), *Thermotoga maritima* (*Tm*SSB) (GenBank^{TM} accession: Q9WZ73), *Deinococcus radiodurans* SSB (*Dr*SSB) (GenBank^{TM} accession: Q9RY51) and *S. cerevisiae* Rim1 (*Sc*Rim1) (GenBank^{TM} accession: AAB22978) are used for the alignment. The sequence alignment determined that the first 100 amino acids from the N-terminal end of Rim1 are involved in formation of the OB-fold domain, and the remaining 18 amino acids from the C-terminal end form the putative unstructured tail region. The amino acid sequences involved in the formation of the C-terminal tails of SSB proteins are highlighted in gray. The C-terminal tail of Rim1 contains five acidic amino acids that are indicated in bold. (**B**) Coomassie blue stained 15% SDS–PAGE gel to visualize purified Rim1 (lane 2) and Rim1ΔC18 (lane 2). The purified proteins were >95% homogenous as assessed from the gel. (**C**) SEC-MALS detection reveals that the Rim1 and Rim1ΔC18 exist as a tetramer. The theoretical MM of monomeric Rim1 and Rim1ΔC18 is 13.29 and 11.43 kDa, respectively. The observed MM and hydrodynamic radius (R_h) for Rim1 and Rim1ΔC18 proteins are as indicated. (**D**) Rim1 binding affinity for ssDNA was evaluated by fluorescence anisotropy. The anisotropy values for Rim1 binding to 1 nM 3′F-T_{20} (open diamonds) and 3′F-T_{70} (closed diamonds) were plotted as average values from three experiments with a standard deviation. Rim1 binding data to 3′F-T_{20} were fit to the Hill equation resulting in a Hill coefficient of 2.5 and an apparent K_d of 3.1 ± 0.1 nM (tetramer). Rim1 binding to 3′F-T_{70} is stoichiometric under the conditions used here (K_d value <1 nM). (**E**) Anisotropy values for binding of Rim1ΔC18 to 1 nM 3′F-T_{20} (open triangles) and 3′F-T_{70} (closed triangles) were plotted as averages from three experiments with a standard deviation. Rim1ΔC18 binding to 3′F-T_{20} was fit to the Hill equation resulting in a Hill coefficient value of 1.6 ± 0.1 and an apparent K_d value of 3.5 ± 0.2 nM (tetramer). Rim1ΔC18 binding to 3′F-T_{70} resulted in two apparent binding modes. A tight binding mode that appears similar to Rim1 (K_d value <1 nM) and a weaker binding mode that did not saturate under these conditions.

relation found between R_h and molar mass for standard globular proteins, indicating a compact globular structure of Rim1ΔC18. However, the R_h value for Rim1 was much higher than the standard globular protein of similar molar mass, indicating that the C-terminal tail exists as an unstructured domain extended away from the core domain.

The ssDNA binding properties of *Ec*SSB and *Hs*mtSSB are well studied (43,50,51). We investigated the Rim1 and Rim1ΔC18 binding to ssDNA by measuring the anisotropy of fluorescein-labeled oligonucleotides. Binding experiments were performed using 3′F-T_{20} and 3′F-T_{70}. Both Rim1 and Rim1ΔC18 bind tightly to 3′F-T_{70} ssDNA (Figure 2D and E). When the data were fit to the quadratic equation, the resulting K_d values were below the concentration of 3′F-T_{70} (1 nM) indicating that binding was stoichiometric under these conditions, suggesting a K_d value of <1 nM. However, Rim1 and Rim1ΔC18 interaction with 3′F-T_{20} is weaker and displays positive cooperativity (Figure 2D and E). By fitting the 3′F-T_{20} binding data for Rim1 and Rim1ΔC18 to the Hill equation, Hill coefficients of 2.5 ± 0.1 and 1.6 ± 0.1 were obtained with apparent K_d values of 3.1 ± 0.1 and 3.5 ± 0.2 nM, respectively.

Direct interaction between Pif1 and Rim1 is mediated through both the OB-fold domain and the C-terminal tail of Rim1

To investigate whether Pif1 and Rim1 interact directly *in vitro*, and to determine whether the C-terminal tail of Rim1 acts as a docking site for interaction between these two proteins, we conducted co-precipitation experiments using two different methods. The first method is a qualitative assay where insolubility of one protein in the presence of ammonium sulfate aids in co-precipitation of the interacting partner. Rim1 exhibited high solubility in ammonium sulfate. The presence of 270 g/l of ammonium sulfate in the reaction efficiently precipitated Pif1 (Figure 3A, compare lane 1 with 11), whereas very little Rim1 (compare lane 3 with 13) or Rim1ΔC18 (lane 7 with 17) protein precipitated under the same conditions. We incubated equimolar amounts of Pif1 and Rim1 protein together in the presence of 270 g/l of ammonium sulfate followed by centrifugation. Most of the Rim1 protein was found in the pellet with Pif1 and no protein was observed in the supernatant fraction (Figure 3A, compare lane 5 with 15). To determine whether the interaction between Pif1 and Rim1 is facilitated through the C-terminal tail of Rim1, a similar co-precipitation experiment was performed by incubating Pif1 and Rim1ΔC18 proteins together. Surprisingly, most of the Rim1ΔC18 protein co-precipitated with Pif1 (Figure 3A, compare lane 9 with 19), indicating that the OB-fold domain of Rim1 is involved in interaction with Pif1.

Interaction between Pif1 and Rim1 was also investigated by covalently linking one of the proteins to epoxy-activated Dynabeads followed by incubation with the other protein. Purified SSB protein was covalently linked to epoxy-activated Dynabeads. Glycine- and BSA-coated beads were used as negative controls. Coated beads were incubated with purified Pif1 protein in a buffer containing 250 mM NaCl. The beads were captured by a magnet and washed five times to remove unbound protein. Pif1 did not co-precipitate with either glycine- or BSA-coated beads (Figure 3B, lane 2 and 3). However, Pif1 was observed to co-precipitate with Rim1-coated beads (Figure 3B, lane 4). To test whether Pif1 and Rim1 co-precipitation is facilitated by DNA, DNase I was included in the reaction but it had no effect on the Pif1–Rim1 interaction (Figure 3B, lane 5). Therefore, co-precipitation between Pif1 and Rim1 is due to protein–protein interactions rather than binding to the same strand of DNA. Pif1 was observed to co-precipitate with Rim1ΔC18 (Figure 3B, lane 7), albeit the amount of Pif1 co-precipitated decreased. To further test the role of OB-fold domain of Rim1 in interaction with Pif1, we included *Hs*mtSSB in the co-precipitation experiments. *Hs*mtSSB shares high homology in the OB-fold domain with Rim1 but exhibits no homology in C-terminal tail region. Pif1 co-precipitated with *Hs*mtSSB-coated beads (Figure 3B, lane 6), although the quantity of Pif1 co-precipitated was less than with Rim1, indicating that the interaction of Pif1 with SSB is partially mediated through the OB-fold domain.

In each experiment utilizing the SSB-coated beads, we observed some SSB protein released from the beads upon heating. This indicates that the subunits of the tetramer are not all covalently linked to the beads. We exploited this observation to normalize the relative amounts of SSBs coated on the beads and then calculated the relative amount of Pif1 co-precipitated with SSB-coated beads. The Pif1 band bound to Rim1 was taken as 1, and the relative amounts of Pif1 co-precipitated with Rim1ΔC18- and *Hs*mtSSB-coated beads was 0.45 and 0.63, respectively (Figure 3C). These results support the conclusion that the OB-fold domain of Rim1 interacts with Pif1, but upon deletion of the C-terminal tail the interaction weakens. The C-terminal tail of Rim1 may act as second interacting site with Pif1.

To further confirm that co-precipitation was due to a direct interaction between the proteins as opposed to binding to the same strand of DNA, all the purified protein preparations were examined for the presence of nucleic acid contamination. All proteins used in this experiment were heat denatured, followed by treatment under conditions that should radiolabel any contaminating DNA with ^{32}P. Analysis of these samples on a denaturing acrylamide gel indicated no contaminating DNA (Supplementary Figure S2A). Furthermore, heat-denatured, purified proteins were resolved on an agarose gel followed by SYBR gold nucleic acid staining which also failed to reveal contaminating DNA (Supplementary Figure S2B).

Pif1 binding affinity to Rim1 is reduced by 3- to 4-fold upon deletion of the C-terminal tail of Rim1

To quantitatively assess the interaction between Pif1 and Rim1, a protein binding fluorescence anisotropy assay was used in which Rim1 was labeled with 5-FAM SE (Figure 4A). The SE form of 5-FAM reacts with amine groups on the protein and forms stable covalent bonds.

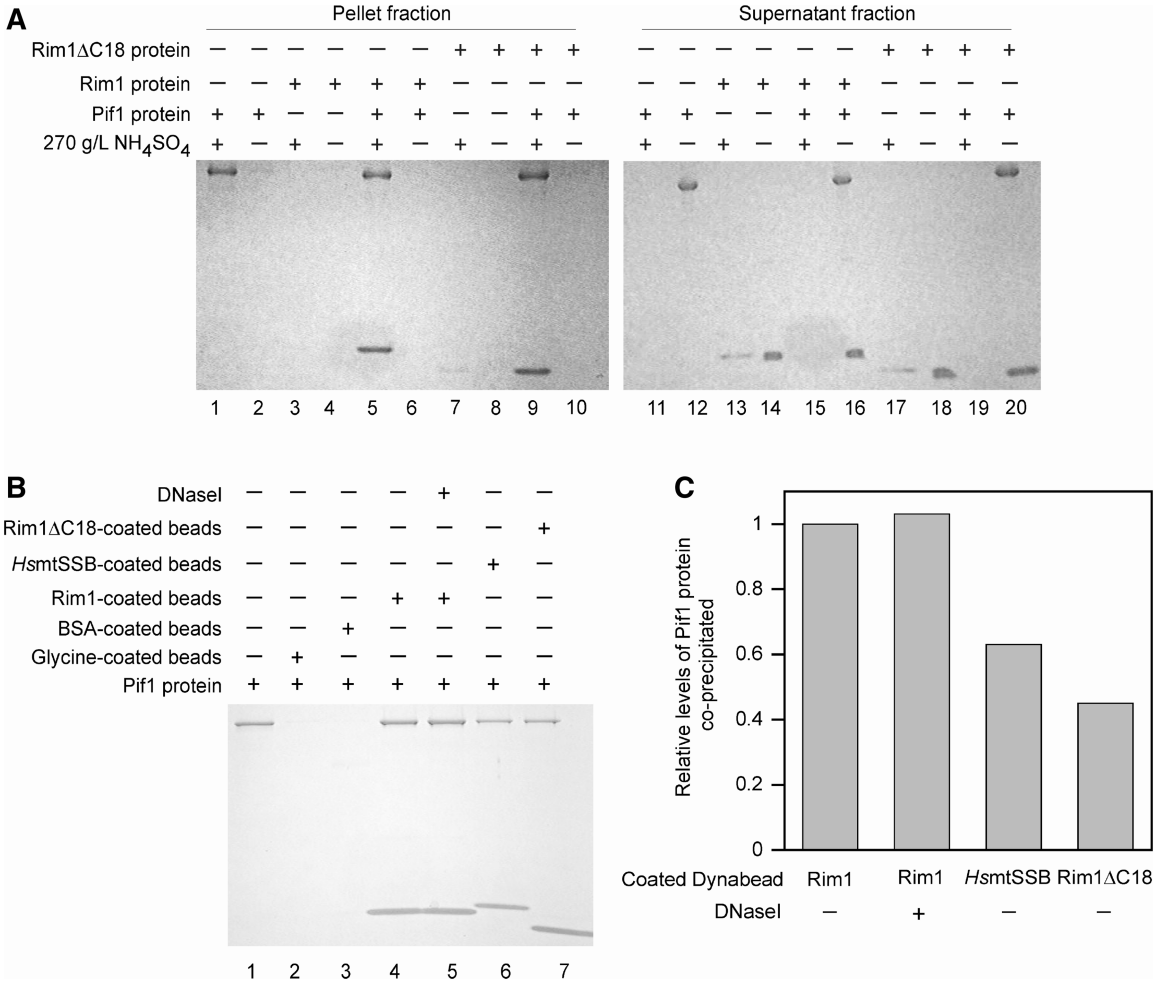

Figure 3. *In vitro* co-precipitation experiments reveal a direct interaction between Rim1 and Pif1 proteins and two possible sites of interactions on Rim1. (**A**) Ammonium sulfate co-precipitation of Pif1 with Rim1 or Rim1ΔC18. The presence of Pif1, Rim1, Rim1ΔC18 and 270 g/l ammonium sulfate in the reaction are indicated by plus symbols. Both pellet and supernatant fractions were analyzed on a 15% SDS–PAGE gel. Rim1 alone (lane 3) or Rim1ΔC18 alone (lane 7) precipitate very little in the presence of ammonium sulfate; however, they co-precipitate completely with Pif1 under the same conditions (lane 5 and 9, respectively). (**B**) Co-precipitation of Pif1 protein with SSB-coated Dynabeads was performed as described in 'Materials and Methods' section. Purified Rim1, Rim1ΔC18 or *Hs*mtSSB protein was coated onto epoxy activated Dynabeads. As a negative control, Dynabeads were coated with glycine or BSA. SSB coated Dynabeads were incubated with equal amounts of purified Pif1. Dynabeads were captured with a magnet, washed and proteins were eluted using SDS–PAGE loading buffer followed by separation on a 4–20% resolving gel. Pif1 did not co-precipitate with glycine-coated (lane 2) or BSA-coated (lane 3) Dynabeads. Pif1 co-precipitated with Rim1-coated beads (lane 4) and its association was not affected in the presence of DNase I (lane 5). Pif1 was also observed to co-precipitate with *Hs*mtSSB-coated (lane 6) and Rim1ΔC18-coated Dynabeads (lane 7). (**C**) A semi-quantitative measurement of relative Pif1 protein association with different SSB-coated Dynabeads from (B). Pif1 protein co-precipitated with each SSB-coated Dynabead was quantified using ImageQuant software and normalized to the amount of SSB protein on the gel. Pif1 association with Rim1-coated beads was taken as 1 and the relative amount of Pif1 co-precipitated with *Hs*mtSSB or Rim1ΔC18-coated beads was 0.63 and 0.45, respectively.

Each molecule of the Rim1 tetramer has 32 lysine amino acids plus four amino terminal ends for reaction with 5-FAM SE. The DOL is the measure of the number of dye molecules per protein molecule. The calculated DOL for 5-FAM labeled Rim1 (FAM-Rim1) was ~8. The DNA binding property of FAM-Rim1 was similar to Rim1 when tested using a TAMRA labeled oligonucleotide (Supplementary Figure S4). FAM-Rim1 exhibited an increase in anisotropy when titrated with unlabeled Rim1 protein (Figure 4B). Subunits of the Rim1 tetramer undergo exchange with labeled Rim1 resulting in a change in anisotropy. Unlabeled *Hs*mtSSB was added to FAM-Rim1, but despite the similarities in the structures of the OB-fold domains, these mtSSBs fail to form cross-species heterotetramers (52). As expected, the anisotropy values did not change when *Hs*mtSSB was titrated into a solution of FAM-Rim1 (Figure 4B). We also prepared 5-FAM labeled Rim1ΔC18 (FAM-Rim1ΔC18). Interestingly, FAM-Rim1ΔC18 did not exhibit a change in anisotropy when titrated with Rim1 or Rim1ΔC18 (data not shown). Rim1ΔC18 may form a more stable tetramer than Rim1, thereby reducing exchange between monomeric units. However, the DNA binding property of FAM-Rim1ΔC18 was similar to unlabeled Rim1ΔC18 protein (Supplementary Figure S4).

Pif1 was titrated into a FAM-Rim1 solution and anisotropy values increased with increasing Pif1 concentration indicating a direct physical interaction between Pif1 and

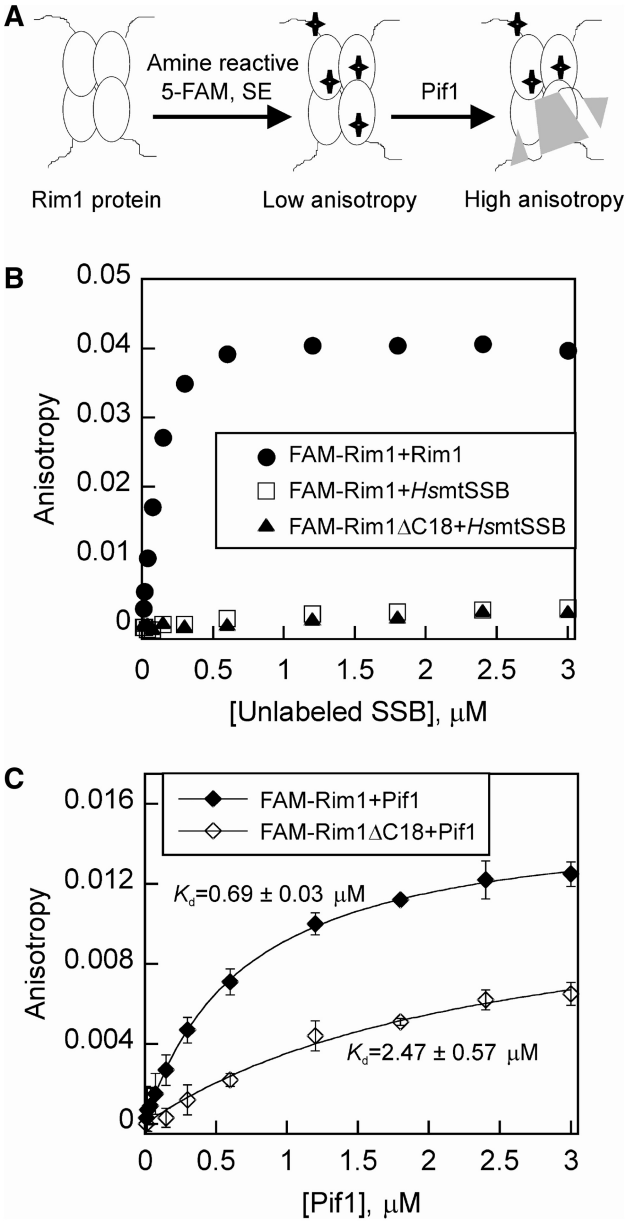

Figure 4. The OB-fold domain and C-terminal tail of Rim1 form two independent Pif1 interaction sites. (**A**) Schematic diagram of the procedure used to measure the binding affinity between Pif1 and SSB protein. Rim1 or Rim1ΔC18 was labeled with the amine reactive fluorescein dye 5-FAM SE as described in 'Materials and Methods' section. The labeled proteins were used in binding assays to measure the change in fluorescence anisotropy as a function of protein binding. (**B**) FAM-labeled Rim1 protein binds to unlabeled Rim1 as indicated by increasing anisotropy; however, it did not bind to *Hs*mtSSB. FAM-labeled Rim1ΔC18 also did not bind to *Hs*mtSSB. (**C**) FAM-labeled Rim1 or FAM-labeled Rim1ΔC18 was titrated with Pif1 protein. The average anisotropy values from at least three independent experiments with a standard deviation were plotted using KaleidaGraph and fit to the equation for a hyperbola to obtain dissociation constants (K_d) of 0.69 ± 0.03 and 2.5 ± 0.6 μM for Pif1 interaction with FAM-Rim1 and FAM-Rim1ΔC18, respectively.

Rim1 (Figure 4C). Changes in the anisotropy values were not as large as normally observed in a protein–DNA binding experiment. This is expected for protein–protein interactions due to the greater MM of labeled Rim1 compared with labeled oligonucleotides. Fitting the anisotropy values to the equation for a hyperbola resulted in a K_d value of 0.69 ± 0.03 μM for Pif1 and FAM-Rim1. To determine the effect of deletion of C-terminal tail of Rim1 on binding affinity, Pif1 was titrated into a solution of FAM-Rim1ΔC18 (Figure 4C). Anisotropy increased with increasing Pif1 concentration indicating interaction between these proteins, however, saturation of binding was not reached due to limiting concentrations of Pif1. Fitting the anisotropy values to a hyperbola yielded a K_d value of 2.5 ± 0.6 μM for Pif1 and FAM-Rim1ΔC18 which was 3- to 4-fold higher than the K_d for the Pif1–Rim1 interaction. These findings are consistent with the results shown in Figure 3 showing the OB-fold domains involvement in interaction with Pif1 and the conclusion that the C-terminal tail acts as a second site for interaction.

Rim1 and Rim1ΔC18 stimulate Pif1 helicase activity

Next, we examined the biochemical significance of the Pif1–Rim1 interaction by measuring Pif1 helicase activity. Previous studies have shown that SSBs can stimulate helicase activity (22,25,27–29,31,53–56). Here, we used two partial duplex DNA substrates that differed by the length of the 5′-loading strand. The substrates, 70T30bp and 20T30bp, had a 30-bp duplex region with a 70-thymidine or 20-thymidine 5′-overhang, respectively (Table 1). Pif1 efficiently unwound both the 70T30bp and 20T30bp substrates with observed rate constants for product formation of 0.44 ± 0.04 and 0.30 ± 0.01 per min, respectively (Figure 5). Rim1 alone failed to unwind either substrate. When Rim1 was preincubated with the 70T30bp substrate before addition of Pif1, a substantial increase in the ssDNA product was observed (Figure 5A and B). The rate constant for product formation was 1.84 ± 0.09 per min in the presence of Rim1, which was more than 4-fold higher than unwinding with Pif1 alone. Preincubation of DNA substrate with Pif1 resulted in faster product formation; however, helicase activity was further stimulated by Rim1 regardless of the order of addition of proteins to the reaction mixture (Supplementary Figure S5).

To test whether reduced interaction between Pif1 and Rim1ΔC18 has any effect on Pif1 helicase activity we substituted Rim1ΔC18 for Rim1 in the reaction. Interestingly, Rim1ΔC18 stimulation of Pif1 helicase activity was only 2-fold (0.90 ± 0.02 per min) (Figure 5A and B). These results indicate that both the OB-fold domain and the C-terminal tail of Rim1 are involved in stimulation of Pif1 helicase activity. In addition, there is a direct correlation between binding affinity between Pif1 and SSBs and their ability to stimulate Pif1 helicase activity. Pif1 unwinding of the 20T30bp substrate was affected very little in the presence of Rim1 (0.31 ± 0.01 per min) or Rim1ΔC18 (0.25 ± 0.01 per min) (Figure 5C and D). This is likely due to the reduced binding of Rim1 and Rim1ΔC18 to the 20 nucleotide ssDNA overhang (Figure 2D and E). The results in Figure 5 indicate that the interaction between Rim1 and Pif1 as well as the interaction between Rim1 and ssDNA are involved in

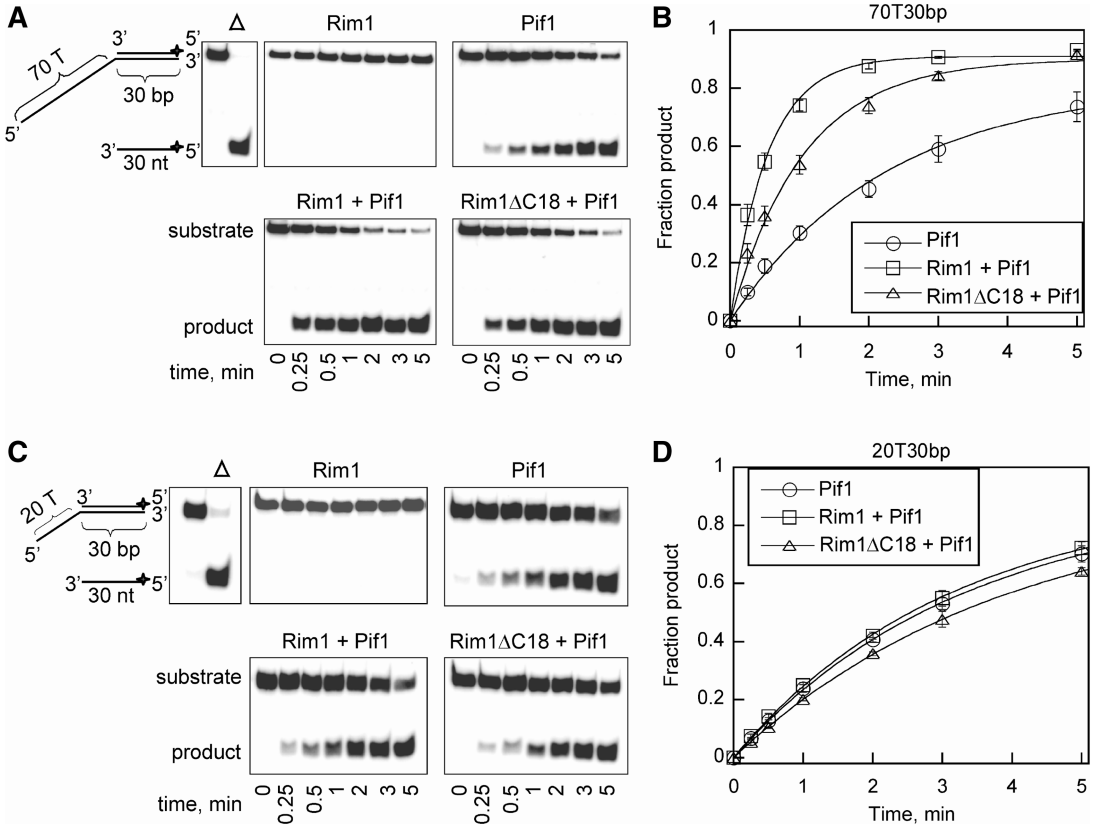

Figure 5. Rim1 and Rim1ΔC18 stimulate Pif1 DNA helicase activity. (**A**) Pif1-catalyzed separation of a partial duplex DNA substrate, 70T30bp, under multiple turnover conditions in the presence or absence of Rim1 or Rim1ΔC18 protein. (**B**) Formation of ssDNA product over time was quantified and plotted as the average of at least three independent reactions with a standard deviation for Pif1 alone (circles), Rim1+Pif1 (squares) and Rim1ΔC18+Pif1 (triangles) from (A). The data were fit to a single exponential resulting in observed rate constants of 0.44 ± 0.04, 1.8 ± 0.1 and 0.90 ± 0.02 per min for Pif1 alone, Rim1+Pif1 and Rim1ΔC18+Pif1, respectively. (**C**) Pif1-catalyzed separation of a partial duplex DNA substrate, 20T30bp, under multiple turnover conditions in the presence or absence of Rim1 or Rim1ΔC18 protein. (**D**) The fraction of ssDNA product formed over time for Pif1 alone (circles), Rim1+Pif1 (squares) and Rim1ΔC18+Pif1 (triangles) from (C) was quantified and plotted as the average of at least three independent reactions with a standard deviation. The observed rate constants for Pif1 alone, Rim1+Pif1 and Rim1ΔC18+Pif1 were 0.30 ± 0.01, 0.31 ± 0.01 and 0.25 ± 0.01 per min, respectively.

stimulation of Pif1 helicase activity. It is known that Pif1 prefers forked DNA substrates over 5′-overhang partial duplex substrates (20). To determine whether stimulation occurred with fork DNA we used a 70T/20T 30 bp substrate for the unwinding experiments. As expected, Pif1 helicase activity was enhanced with the fork substrate compared to the single-stranded overhang (Supplementary Figure S6). Pif1 unwinding activity of the fork substrate was further stimulated by ~3-fold in the presence of Rim1 (Supplementary Figure S6).

Effect of heterologous SSB proteins on Pif1 catalyzed unwinding activity

To determine whether the stimulation of Pif1 helicase is due to binding of released ssDNA product by SSB, two heterologous SSB proteins *Hs*mtSSB and gp32 (from bacteriophage T4) were examined. *Hs*mtSSB, like Rim1, exists as a stable tetramer, whereas gp32 is a monomer that binds to ssDNA with high cooperativity (45,57). Study of ssDNA binding affinity of *Hs*mtSSB and gp32 with 3′F-T_{20} and 3′F-T_{70} revealed that *Hs*mtSSB binds with similar affinity as Rim1, whereas gp32 showed somewhat weaker binding (Supplementary Figure S3). Pif1 strand separation activity of 70T30bp was stimulated by 2- to 3-fold in the presence of *Hs*mtSSB (1.14 ± 0.13 per min) (Figure 6A). This data correlates well with the *in vitro* co-precipitation experiment showing the interaction between Pif1 and *Hs*mtSSB protein through the OB-fold domain in a manner similar to Rim1ΔC18 (Figure 3B and C). *Hs*mtSSB and Rim1ΔC18 result in comparable enhancements in the rate of Pif1 unwinding and have similar affinities for Pif1. As gp32 has a smaller binding site size of 7 nt per unit compared with tetrameric SSBs, we used a 5-fold excess of gp32 in the reaction. Interestingly, gp32 had little effect on Pif1 helicase activity with the 70T30bp substrate (0.58 ± 0.02 per min) (Figure 6A), indicating that sequestering of released product by SSBs does not increase product formation under these conditions. Rather, direct interaction with Pif1 is required for stimulation of Pif1 helicase activity. Pif1 strand separation activity with the 20T30bp substrate was not strongly affected in the presence of *Hs*mtSSB or gp32 (Figure 6B). Hence, the 20 nt loading strand does not support SSB stimulation of Pif1 activity.

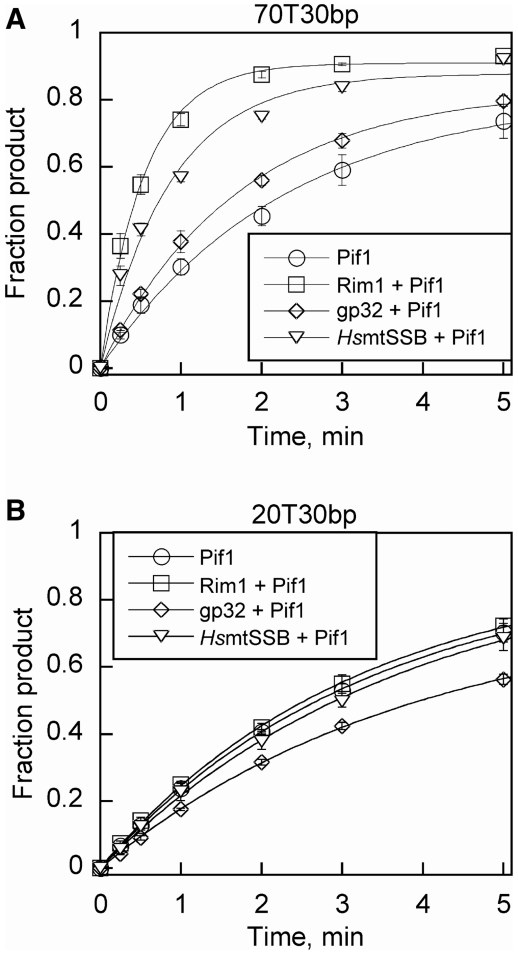

Figure 6. Effect of heterologous SSBs on Pif1-catalyzed DNA helicase activity. (**A**) The fraction of ssDNA product formed under multiple turnover conditions with the 70T30bp substrate for *Hs*mtSSB+Pif1 (triangles), and gp32+Pif1 (diamonds) was plotted as the average value of three independent experiments along with Pif1 alone (circles) and Rim1+Pif1 (squares) which is replotted for comparison from Figure 5B. The data were fit to a single exponential resulting in observed rate constants for product formation of 0.44 ± 0.04, 1.84 ± 0.09, 1.1 ± 0.1 and 0.58 ± 0.02 per min for Pif1 alone, Rim1+Pif1, *Hs*mtSSB+Pif1 and gp32+Pif1, respectively. (**B**) Results of DNA strand separation experiments conducted with the 20T30bp substrate. The fraction of ssDNA formed over time for Pif1 alone (circles), Rim1+Pif1 (squares), *Hs*mtSSB+Pif1 (triangles) and gp32+Pif1 (diamonds) was plotted as the average of at least three independent experiments. The observed rate constants for Pif1 alone, Rim1+Pif1, *Hs*mtSSB+Pif1 and gp32+Pif1 were 0.30 ± 0.01, 0.31 ± 0.01, 0.26 ± 0.02 and 0.25 ± 0.01 per min, respectively.

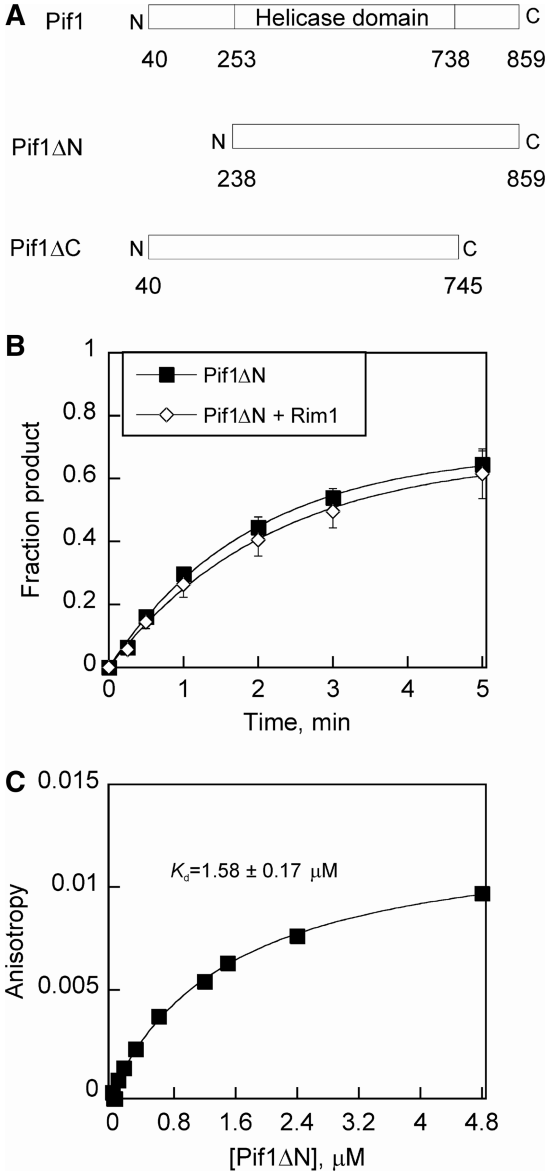

Figure 7. The N-terminal domain of Pif1 is essential for Rim1 mediated stimulation of helicase activity. (**A**) Schematic diagram of the Pif1 variants used: the N-terminal deletion mutant (Pif1ΔN) and the C-terminal deletion mutant (Pif1ΔC). (**B**) Results of Pif1ΔN-catalyzed separation of a partial duplex DNA substrate, 70T30bp, under multiple turnover conditions in the presence or absence of Rim1. The fraction of ssDNA formed over time for Pif1ΔN (closed squares) and Pif1ΔN+Rim1 (open diamonds) was plotted as the average of at least three independent experiments. The observed rate constants for Pif1ΔN and Pif1ΔN+Rim1 were 0.52 ± 0.03 and 0.46 ± 0.03 per min, respectively. (**C**) Binding affinity of Pif1ΔN with FAM-Rim1. Fluorescence anisotropy of FAM-Rim1 was plotted as a function of increasing concentrations of Pif1ΔN. Data were fit to the equation for a hyperbola to obtain a K_d value of $1.6 \pm 0.2\,\mu M$.

Mapping the interaction site on Pif1 reveals that the N-terminal domain is essential for the stimulation of helicase activity

Pif1 can be broadly divided into three domains: the N-terminal domain, helicase domain and C-terminal domain (Figure 7A). The helicase domain is essential for DNA strand separation activity in an ATP-dependent manner. The roles of the N-terminal or C-terminal domains of Pif1 are unknown. To determine the effect of the N-terminal or C-terminal domain of Pif1 on Rim1 stimulated helicase activity, we purified Pif1ΔN and Pif1ΔC to homogeneity (Supplementary Figure S1B). Measurement of the ATPase activity showed that Pif1ΔN was similar to Pif1, whereas Pif1ΔC did not show any activity (Supplementary Figure S1C). Pif1ΔC also did not show any ssDNA binding activity

(data not shown), hence the C-terminal mutant was not further characterized.

The helicase activity of Pif1ΔN was comparable to full-length Pif1 (Figures 5B and 7B). Surprisingly, addition of Rim1 to the reaction did not stimulate Pif1ΔN strand separation activity (Figure 7B). The observed rate constants for product formation with Pif1ΔN alone and in the presence of Rim1 were 0.52 ± 0.03 and 0.46 ± 0.03 per min, respectively. These results indicate that the N-terminal domain of Pif1 is essential for the stimulation of Pif1-catalyzed strand separation activity by Rim1. Titration of FAM-Rim1 with Pif1ΔN resulted in a change in anisotropy (Figure 7C). Fitting the data to a hyperbola yielded a K_d value of 1.6 ± 0.2 μM indicating that the interaction between Pif1ΔN and Rim1 protein was not lost completely. However, the binding affinity between Pif1ΔN and Rim1 was reduced by ~2.5-fold when compared with the Pif1 and Rim1 interaction (Figures 4C and 7C). The results are consistent with Pif1 having two sites for interaction with Rim1, one in the N-terminal domain and the other in the helicase domain or in the C-terminal domain.

Rim1 does not stimulate the Pif1 ATPase activity

To address the possible mechanism of Rim1 stimulation of Pif1 helicase activity, we measured the effect of Rim1 on ssDNA-dependent ATPase activity of Pif1 (Figure 8A and B). The k_{cat} value for Pif1 ATPase activity was 95 ± 5 per s with saturating concentration of poly(dT) and this value was similar in the presence of Rim1 (97 ± 2 per s). The K_{eff} value reflects the concentration of ssDNA needed to achieve half the maximum ATPase activity. The K_{eff} value for Pif1 ATPase hydrolysis was 1.1 ± 0.2 μM, which was slightly higher than previously published data of ~0.6 μM (17). However, the K_{eff} value was ~3-fold higher (3.4 ± 0.2 μM) in the presence of Rim1, which may reflect simple competition for binding to the ssDNA. The k_{cat} for ATP hydrolysis for Pif1 at saturating concentrations of poly(dT) was determined with increasing concentrations of Rim1, but no effect on the Pif1 ATPase activity was observed (Figure 8B). From these results, we conclude that stimulation of Pif1 helicase activity is not due to an increased rate of ATP hydrolysis.

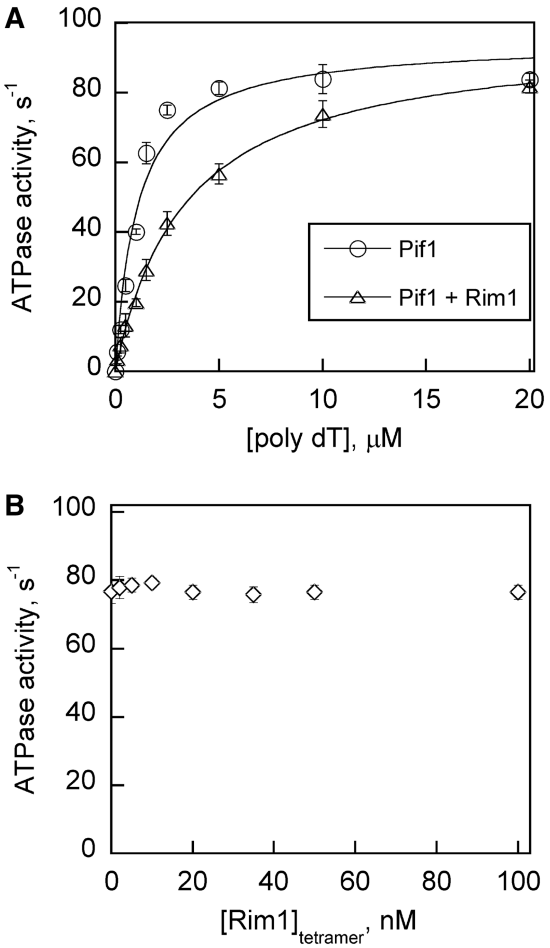

Figure 8. Rim1 has no effect on the k_{cat} value for ATP hydrolysis catalyzed by Pif1. (**A**) DNA stimulated ATPase activity of Pif1 (100 nM) in the presence or absence of Rim1 (100 nM) at increasing concentrations of poly(dT). The ATPase activity of Pif1 was plotted as the average value from three independent experiments and data were fit to a hyperbola to obtain kinetic constants k_{cat} and K_{eff}. The observed k_{cat} value for Pif1 was 94.7 ± 4.9 per s and it did not change in the presence of Rim1 (96.7 ± 1.8 per s). The measured K_{eff} value for Pif1 was 1.07 ± 0.2 μM and it increased by 3-fold in the presence of Rim1 (3.4 ± 0.2 μM). (**B**) DNA-stimulated Pif1 (20 nM) ATPase activity at saturating concentrations of poly(dT) (20 μM) was measured with increasing concentrations of Rim1. The average Pif1 ATPase activity from three independent experiments was plotted. Titration with Rim1 had no effect on Pif1 ATPase activity.

DISCUSSION

The Pif1 helicase is crucial for several different cellular processes, suggesting that its activity may be modulated through its interaction with other proteins. Numerous helicases from both prokaryotes and eukaryotes are known to interact with other proteins in a manner that regulates helicase activity (22,25,27–29,31,53–56). Previous efforts to determine the Pif1 interactome have used tagged protein as bait in a high-throughput global analysis of protein–protein interactions in *S. cerevisiae* (36,58,59), but none of these studies have reported any interactors for Pif1. However, Pif1 was identified as one of the hits in a high-throughput affinity capture experiment where Nab2 (60), Cct3 (61) and Dsn1 (62) were used as bait. One problem associated with affinity-tag capture methods is co-enrichment of nonspecific interactors, i.e. false positive results. To overcome this problem, researchers often increase the stringency for affinity capture, but this can result in a loss of specific interactions, i.e. false-negative results.

High-throughput methods are increasingly being replaced by more focused analyses of protein–protein interactions. A modified method for targeted affinity capture followed by MS called I-DIRT can differentiate specific protein interactions from nonspecific (37). This technique primarily differs from traditional affinity capture-MS method in growing the cells in isotopic media and in analyzing the MS results. A recent report on the identification of the NuA3 acetyltransferase interactome using the I-DIRT technique showed that

278 proteins of 288 proteins identified were actually nonspecific interactors (63). We employed this technique to determine the specific interacting partners for Pif1. We identified Pif1 interactions with 23 proteins by analyzing the data for normal affinity capture, however, when the data were analyzed using the I-DIRT method, we found one specific protein interaction with Pif1, a mitochondrial SSB called Rim1 (Figure 1). We observed this Pif1–Rim1 interaction in four independent affinity capture experiments.

Several reports on the Rim1 interactome have identified protein interactions using the yeast two-hybrid system (64), high-throughput affinity capture-MS methods (35,36,58) and a protein-fragment complementation assay (59). However, none of these studies have identified its interaction with Pif1. Protein interactions have been identified between Rim1 and key mitochondrial proteins which are involved in DNA repair (35,36,58,65,66). These proteins include Apn1, an apurinic/apyrimidinic endonuclease involved in base excision repair (67), Rad52, a protein involved in double-strand DNA break repair and homologous recombination (68), Mgm101, a protein involved in repair of oxidative mtDNA damage (69) and Dna2, a protein involved in Okazaki fragment maturation and DNA repair (70). Functional characterization of these putative interactions has yet to be reported.

Yeast mtDNA is generally classified into three different types, rho^+ (wt mtDNA), rho^- (large deletions in mtDNA) and rho^0 (completely devoid of mtDNA) (71). Both Pif1 and Rim1 are involved in maintenance of mtDNA (4–9,72). Interestingly, Rim1 was originally discovered as a multicopy suppressor of a heat-sensitive phenotype of the *pif1* null mutant (6). At elevated growth temperatures, *pif1* null mutant strains lose their mitochondrial genome and do not grow on a nonfermentable media, however, this phenotype can be partially rescued by overexpression of Rim1. A *rim1* null mutant completely lost its mitochondrial genome, even when cells were grown on a nonfermentable carbon source (6). Pif1 was first described as a mtDNA helicase involved in stimulation of recombination between rho^+ and rho^- mtDNA (4,5). *pif1* null mutant strains exhibited increased frequency of recombination between rho^+ and tandemly organized rho^- mtDNA genomes resulting in a higher rate of spontaneous rho^0 mutant formation. Additional experiments with *pif1* null mutations indicated that Pif1 is involved in inhibition/repair of spontaneous oxidative damage of mtDNA (8,73). Absence of mitochondrial Pif1 is also associated with a decrease in mtDNA copy number (74), functional loss of mitochondria and fragmentation of mtDNA in the presence of the genotoxic chemical ethidium bromide (79). Studies on both Pif1 and Rim1 have showed that they are involved in maintenance of the mitochondrial genome. Often DNA helicases and SSB proteins have been observed to perform complementary functions in many aspects of DNA metabolism (22,28,29,56).

It is possible that affinity tag methods indicate indirect protein–protein interactions that could be due to both proteins being a part of the same protein complex. Alternatively, the interaction may occur through the tag used for the pull-down experiment, or it may occur through a strand of DNA to which both the proteins are associated. Direct interaction between Pif1 and Rim1 was examined using purified proteins. Both the proteins were characterized for their known functions (Figure 2; Supplementary Figure S1) and checked for DNA contamination before proceeding with *in vitro* interaction experiments (Supplementary Figure S2). Two co-precipitation methods were used to confirm the interaction between these two proteins. Both the methods showed a direct physical interaction between Pif1 and Rim1 *in vitro*, confirming results from the *in vivo* interaction determined by the TAP-tag pull-down (Figure 3).

To determine the structural regions from each protein that support the Pif1-Rim1, truncated variant proteins and two heterologous SSB proteins were purified. The C-terminal tail region in *Ec*SSB acts as the docking site for several proteins which is mediated through a conserved acidic amino acid sequence (DDDIPF) (22,49). We found that deletion of the C-terminal tail of Rim1 (Rim1ΔC18) partially disrupted the *in vitro* interaction with Pif1 (Figure 3). This indicated that both the C-terminal tail, as in *Ec*SSB, and the OB-fold domain, are involved in interaction with Pif1. We further confirmed the Pif1–Rim1 interaction through the OB-fold domain by observing a direct interaction between *Hs*mtSSB and Pif1 in an *in vitro* co-precipitation experiment (Figure 3B). *Hs*mtSSB and Rim1 share high homology in the OB-fold domain and are expected to form similar structures, however, their C-terminal tails are unique. Interestingly, the association between *Hs*mtSSB and Twinkle helicase in human mitochondria occurs through the OB-fold domains, demonstrating that these domains serve as a scaffold for protein interactions in addition to their role in DNA binding (75,76). Studies on the BLM helicase complex revealed that multiple OB-fold domains participate through two modes of action: protein–DNA interaction through RPA and protein–protein interactions through RMI (76).

Although deletion of the C-terminal tail of Rim1 did not completely disrupt the interaction with Pif1, the association appeared weaker than full length Rim1 (Figure 3B and C). To quantitatively estimate the affinity between the proteins we used a protein fluorescence anisotropy assay. Results for Pif1 and FAM-Rim1 binding indicated an affinity between these two proteins of 0.69 μM (Figure 4C). This is ~10-fold stronger than the reported interaction between *E. coli* RecQ and *Ec*SSB (K_d of 6 μM), which is solely mediated through the C-terminal tail of the SSB. An anisotropy assay using Pif1 and FAM-Rim1ΔC18 indicated that the affinity between these proteins is decreased 3- to 4-fold relative to full length Rim1 (K_d of 2.5 μM) (Figure 4C). This indicated that both the OB-fold domain and the C-terminal tail of Rim1 posses unique binding sites on Pif1. An N-terminal deletion of Pif1 (Pif1ΔN) was used to map part of the interaction site with Rim1. We observed that association of Pif1ΔN with Rim1 was decreased by ~2.5-fold (K_d of 1.6 μM) (Figure 7C). This indicated that the N-terminal domain of Pif1 acts as one of the two interaction sites for Rim1. Failure to observe any stimulation in Pif1ΔN

helicase activity in the presence of Rim1 indicated that interaction with the N-terminal domain of Pif1 is essential for the stimulation of helicase activity.

Reports on several helicase-SSB interactions showed increased helicase processivity in the presence of SSBs (54,77,78). Two known helicases interacting with *Ec*SSB through the C-terminal tail are RecQ and PriA helicases, both of which exhibit enhanced helicase activity in the presence of *Ec*SSB (22,79). Mutations in the OB-fold domain of *Hs*mtSSB resulted in reduced stimulation of Twinkle helicase activity, indicating that direct interaction between these two proteins is necessary for stimulation of helicase activity (44). Twinkle helicase is not only stimulated by *Hs*mtSSB but also stimulated by *Ec*SSB, and *Dm*mtSSB (*D. melanogaster* mtSSB) which have similar OB-fold domains but distinct C-terminal tails (44). We observed a similar stimulation for Pif1 helicase activity in the presence of *Hs*mtSSB (Figure 6A).

We observed a 4- to 5-fold increase in Pif1-catalyzed strand separation activity in the presence of Rim1 with a substrate that contained a 70 nt overhang (Figure 5A and B). Rim1 provided no stimulation with a substrate containing a 20 nt overhang (Figure 5C and D). Rim1 binds much more tightly to a 70mer than to a 20mer (Figure 2D). The strong interaction between Pif1 and Rim1 and the tight association between Rim1 and the long ssDNA overhang may allow the SSB to function as a processivity factor. Examining the Pif1 helicase activity in the presence of Rim1ΔC18 showed ~2-fold higher activity than Pif1 alone (Figure 5A and B). Deletion of the Rim1 C-terminal tail had little effect on ssDNA binding affinity (Figure 2E). This indicated that the Pif1 interaction with the Rim1 OB-fold domain is important for stimulation of helicase activity. In addition, the C-terminal tail of Rim1 also appears to interact with Pif1. These results are in contrast with RecQ and an *Ec*SSB C-terminal tail deletion variant which strongly inhibited helicase activity. A report on Pif1 has shown that RPA stimulates its helicase activity *in vitro* (20). RPA is a heterotrimeric nuclear SSB protein that binds tightly to ssDNA through interactions with a series of OB-fold domains (80). It is possible that RPA interacts with Pif1 through the OB-fold domains in a manner similar to Rim1.

In vitro stimulation of helicase activity by SSBs can be envisioned to occur through protein interactions whereby the SSB holds the helicase onto the DNA, similar to a processivity factor. Alternatively, the SSB might increase helicase function by providing a binding site for ssDNA as it emerges from the helicase, thereby preventing reannealing. SSB binding to ssDNA might also create a high affinity site for association of the helicase with the DNA. The Pif1 ATPase activity was not changed in the presence Rim1 (Figure 8). It appears that the stimulation of Pif1 helicase activity is directly modulated based on the binding affinity with SSB protein. However, the precise mechanism for Rim1 stimulation of Pif1 unwinding activity requires further investigation.

The specific roles *in vivo* for the Pif1–Rim1 interaction remain to be determined. The importance of each individual protein in mtDNA maintenance has been established, so the *in vivo* and *in vitro* results reported here indicate that the protein interaction likely regulates their activities in mitochondria. A recent report on Pif1 demonstrated that it is bound to the mitochondrial inner membrane as part of a ~900 kDa protein complex containing Mip1 (equivalent to the human mtDNA pol γ) and Abf2 (81). Abf2 is a mtDNA-binding protein involved in replication and recombination (82). Rim1 has been proposed to function as a component of the yeast mtDNA replisome in a manner similar to *Hs*mtSSB in human mitochondria. As Pif1 can only unwind short DNA substrates *in vitro* due to low processivity, it has been proposed to perform a nonessential role in mtDNA replication (9). Twinkle helicase can only unwind short stretches of dsDNA when examined alone, indicating low processivity (31). However, it forms part of the processive replicative machinery in combination with *Hs*mtSSB and pol γ (33,34). Thus far, the yeast helicase responsible for replicative mtDNA synthesis has not been identified and the yeast genome does not encode a close homolog of Twinkle helicase. Another mitochondrial helicase, Hmi1, was initially proposed to be the replicative helicase in yeast mitochondria based on its role in maintenance of the rho^+ genome but not the rho^- genome (83). However, additional studies showed that Hmi1 lacking ATPase activity can still support the maintenance of rho^+ genome, indicating that a different DNA helicase can support mtDNA replication (84). Replicative helicases are typically hexameric, ring-shaped enzymes, although the dimeric herpesvirus helicase can fulfill this role (85,86). Pif1 was shown to exist as monomer in solution but can dimerize upon binding to ssDNA (19). Interaction of Rim1 with Pif1 may play roles in replication functions at G4 quadruplex DNA structures and stalled DNA replication folks, which Pif1 is known to resolve (16,87,88). A recent report on Pif1 showed that nuclear DNA replication through G4 motifs is promoted by the Pif1 helicase (89). Although the yeast mitochondrial genome is highly AT-rich, it has nearly 10-fold higher density of G4 motifs than nuclear DNA (90). It is possible that the Pif1–Rim1 interaction is necessary for the recruitment of Pif1 into the active replication complex to resolve G4 structures. In light of the varied, individual roles played by Pif1 and Rim1 in maintenance of mtDNA, it is likely that the interaction between these two proteins modulates these functions.

SUPPLEMENTARY DATA

Supplementary Data are available at NAR Online: Supplementary Table 1, Supplementary Figures 1–6 and Supplementary Materials and Methods.

ACKNOWLEDGEMENTS

We acknowledge UAMS Proteomics Core Facility for mass spectrometry. We thank Dr Alicia K. Byrd for critical reading of the manuscript. We also thank Dr Robert L. Eoff for assistance with the SEC-MALS experiments.

FUNDING

Funding for open access charge: National Institutes of Health (NIH) [R01 GM098922 to K.D.R.]; NIH [COBRE P20RR015569 (F. Millett, P.I.), R01 DA025755 to A.J.T.]; Award Number UL1RR029884 from the NIH National Center for Research Resources and National Center for Advancing Translational Sciences (to C. Lowery, P.I.).

Conflict of interest statement. None declared.

REFERENCES

1. Bochman,M.L., Sabouri,N. and Zakian,V.A. (2010) Unwinding the functions of the Pif1 family helicases. *DNA Repair (Amst.)*, **9**, 237–249.
2. Bessler,J.B., Torredagger,J.Z. and Zakian,V.A. (2001) The Pif1p subfamily of helicases: region-specific DNA helicases? *Trends Cell Biol.*, **11**, 60–65.
3. Zhou,J., Monson,E.K., Teng,S.C., Schulz,V.P. and Zakian,V.A. (2000) Pif1p helicase, a catalytic inhibitor of telomerase in yeast. *Science*, **289**, 771–774.
4. Foury,F. and Kolodynski,J. (1983) pif mutation blocks recombination between mitochondrial rho+ and rho- genomes having tandemly arrayed repeat units in *Saccharomyces cerevisiae*. *Proc. Natl Acad. Sci. USA*, **80**, 5345–5349.
5. Foury,F. and Dyck,E.V. (1985) A PIF-dependent recombinogenic signal in the mitochondrial DNA of yeast. *EMBO J.*, **4**, 3525–3530.
6. Van,D.E., Foury,F., Stillman,B. and Brill,S.J. (1992) A single-stranded DNA binding protein required for mitochondrial DNA replication in *S. cerevisiae* is homologous to *E. coli* SSB. *EMBO J.*, **11**, 3421–3430.
7. Cheng,X., Dunaway,S. and Ivessa,A.S. (2007) The role of Pif1p, a DNA helicase in *Saccharomyces cerevisiae*, in maintaining mitochondrial DNA. *Mitochondrion*, **7**, 211–222.
8. O'Rourke,T.W., Doudican,N.A., Mackereth,M.D., Doetsch,P.W. and Shadel,G.S. (2002) Mitochondrial dysfunction due to oxidative mitochondrial DNA damage is reduced through cooperative actions of diverse proteins. *Mol. Cell. Biol.*, **22**, 4086–4093.
9. Cheng,X., Qin,Y. and Ivessa,A.S. (2009) Loss of mitochondrial DNA under genotoxic stress conditions in the absence of the yeast DNA helicase Pif1p occurs independently of the DNA helicase Rrm3p. *Mol. Genet. Genomics*, **281**, 635–645.
10. Boule,J.B., Vega,L.R. and Zakian,V.A. (2005) The yeast Pif1p helicase removes telomerase from telomeric DNA. *Nature*, **438**, 57–61.
11. Schulz,V.P. and Zakian,V.A. (1994) The saccharomyces PIF1 DNA helicase inhibits telomere elongation and de novo telomere formation. *Cell*, **76**, 145–155.
12. Myung,K., Chen,C. and Kolodner,R.D. (2001) Multiple pathways cooperate in the suppression of genome instability in *Saccharomyces cerevisiae*. *Nature*, **411**, 1073–1076.
13. Budd,M.E., Reis,C.C., Smith,S., Myung,K. and Campbell,J.L. (2006) Evidence suggesting that Pif1 helicase functions in DNA replication with the Dna2 helicase/nuclease and DNA polymerase delta. *Mol. Cell. Biol.*, **26**, 2490–2500.
14. Rossi,M.L., Pike,J.E., Wang,W., Burgers,P.M., Campbell,J.L. and Bambara,R.A. (2008) Pif1 helicase directs eukaryotic Okazaki fragments toward the two-nuclease cleavage pathway for primer removal. *J. Biol. Chem.*, **283**, 27483–27493.
15. Ivessa,A.S., Zhou,J.Q. and Zakian,V.A. (2000) The Saccharomyces Pif1p DNA helicase and the highly related Rrm3p have opposite effects on replication fork progression in ribosomal DNA. *Cell*, **100**, 479–489.
16. Ribeyre,C., Lopes,J., Boule,J.B., Piazza,A., Guedin,A., Zakian,V.A., Mergny,J.L. and Nicolas,A. (2009) The yeast Pif1 helicase prevents genomic instability caused by G-quadruplex-forming CEB1 sequences in vivo. *PLoS Genet.*, **5**, e1000475.
17. Lahaye,A., Leterme,S. and Foury,F. (1993) PIF1 DNA helicase from *Saccharomyces cerevisiae*. Biochemical characterization of the enzyme. *J. Biol. Chem.*, **268**, 26155–26161.
18. Singleton,M.R., Dillingham,M.S. and Wigley,D.B. (2007) Structure and mechanism of helicases and nucleic acid translocases. *Annu. Rev. Biochem.*, **76**, 23–50.
19. Barranco-Medina,S. and Galletto,R. (2010) DNA binding induces dimerization of *Saccharomyces cerevisiae* Pif1. *Biochemistry*, **49**, 8445–8454.
20. Boule,J.B. and Zakian,V.A. (2007) The yeast Pif1p DNA helicase preferentially unwinds RNA DNA substrates. *Nucleic Acids Res.*, **35**, 5809–5818.
21. Makovets,S. and Blackburn,E.H. (2009) DNA damage signalling prevents deleterious telomere addition at DNA breaks. *Nat. Cell Biol.*, **11**, 1383–1386.
22. Shereda,R.D., Bernstein,D.A. and Keck,J.L. (2007) A central role for SSB in *Escherichia coli* RecQ DNA helicase function. *J. Biol. Chem.*, **282**, 19247–19258.
23. Lachapelle,S., Gagne,J.P., Garand,C., Desbiens,M., Coulombe,Y., Bohr,V.A., Hendzel,M.J., Masson,J.Y., Poirier,G.G. and Lebel,M. (2011) Proteome-wide identification of WRN-interacting proteins in untreated and nuclease-treated samples. *J. Proteome. Res.*, **10**, 1216–1227.
24. Laursen,L.V., Bjergbaek,L., Murray,J.M. and Andersen,A.H. (2003) RecQ helicases and topoisomerase III in cancer and aging. *Biogerontology*, **4**, 275–287.
25. Schwendener,S., Raynard,S., Paliwal,S., Cheng,A., Kanagaraj,R., Shevelev,I., Stark,J.M., Sung,P. and Janscak,P. (2010) Physical interaction of RECQ5 helicase with RAD51 facilitates its anti-recombinase activity. *J. Biol. Chem.*, **285**, 15739–15745.
26. Lu,D., Myers,A.R., George,N.P. and Keck,J.L. (2011) Mechanism of Exonuclease I stimulation by the single-stranded DNA-binding protein. *Nucleic Acids Res.*, **39**, 6536–6545.
27. Ahn,B., Lee,J.W., Jung,H., Beck,G. and Bohr,V.A. (2009) Mechanism of Werner DNA helicase: POT1 and RPA stimulates WRN to unwind beyond gaps in the translocating strand. *PLoS One*, **4**, e4673.
28. Machwe,A., Lozada,E., Wold,M.S., Li,G.M. and Orren,D.K. (2011) Molecular cooperation between the Werner syndrome protein and replication protein A in relation to replication fork blockage. *J. Biol. Chem.*, **286**, 3497–3508.
29. Cadman,C.J. and McGlynn,P. (2004) PriA helicase and SSB interact physically and functionally. *Nucleic Acids Res.*, **32**, 6378–6387.
30. Huang,C.Y., Hsu,C.H., Sun,Y.J., Wu,H.N. and Hsiao,C.D. (2006) Complexed crystal structure of replication restart primosome protein PriB reveals a novel single-stranded DNA-binding mode. *Nucleic Acids Res.*, **34**, 3878–3886.
31. Korhonen,J.A., Gaspari,M. and Falkenberg,M. (2003) TWINKLE Has 5′ -> 3′ DNA helicase activity and is specifically stimulated by mitochondrial single-stranded DNA-binding protein. *J. Biol. Chem.*, **278**, 48627–48632.
32. Baloh,R.H., Salavaggione,E., Milbrandt,J. and Pestronk,A. (2007) Familial parkinsonism and ophthalmoplegia from a mutation in the mitochondrial DNA helicase twinkle. *Arch. Neurol.*, **64**, 998–1000.
33. Jemt,E., Farge,G., Backstrom,S., Holmlund,T., Gustafsson,C.M. and Falkenberg,M. (2011) The mitochondrial DNA helicase TWINKLE can assemble on a closed circular template and support initiation of DNA synthesis. *Nucleic Acids Res.*, **39**, 9238–9249.
34. Korhonen,J.A., Pham,X.H., Pellegrini,M. and Falkenberg,M. (2004) Reconstitution of a minimal mtDNA replisome in vitro. *EMBO J.*, **23**, 2423–2429.
35. Gavin,A.C., Bosche,M., Krause,R., Grandi,P., Marzioch,M., Bauer,A., Schultz,J., Rick,J.M., Michon,A.M., Cruciat,C.M. *et al.* (2002) Functional organization of the yeast proteome by systematic analysis of protein complexes. *Nature*, **415**, 141–147.
36. Krogan,N.J., Cagney,G., Yu,H., Zhong,G., Guo,X., Ignatchenko,A., Li,J., Pu,S., Datta,N., Tikuisis,A.P. *et al.* (2006) Global landscape of protein complexes in the yeast *Saccharomyces cerevisiae*. *Nature*, **440**, 637–643.
37. Tackett,A.J., DeGrasse,J.A., Sekedat,M.D., Oeffinger,M., Rout,M.P. and Chait,B.T. (2005) I-DIRT, a general method for

distinguishing between specific and nonspecific protein interactions. *J. Proteome Res.*, **4**, 1752–1756.
38. Marblestone,J.G., Edavettal,S.C., Lim,Y., Lim,P., Zuo,X. and Butt,T.R. (2006) Comparison of SUMO fusion technology with traditional gene fusion systems: enhanced expression and solubility with SUMO. *Protein Sci.*, **15**, 182–189.
39. Deng,X., Prakash,A., Dhar,K., Baia,G.S., Kolar,C., Oakley,G.G. and Borgstahl,G.E. (2009) Human replication protein A-Rad52-single-stranded DNA complex: stoichiometry and evidence for strand transfer regulation by phosphorylation. *Biochemistry*, **48**, 6633–6643.
40. Jennings,T.A., Mackintosh,S.G., Harrison,M.K., Sikora,D., Sikora,B., Dave,B., Tackett,A.J., Cameron,C.E. and Raney,K.D. (2009) NS3 helicase from the hepatitis C virus can function as a monomer or oligomer depending on enzyme and substrate concentrations. *J. Biol. Chem.*, **284**, 4806–4814.
41. Sikora,B., Eoff,R.L., Matson,S.W. and Raney,K.D. (2006) DNA unwinding by *Escherichia coli* DNA helicase I (TraI) provides evidence for a processive monomeric molecular motor. *J. Biol. Chem.*, **281**, 36110–36116.
42. Raney,K.D. and Benkovic,S.J. (1995) Bacteriophage T4 Dda helicase translocates in a unidirectional fashion on single-stranded DNA. *J. Biol. Chem.*, **270**, 22236–22242.
43. Ferrari,M.E., Bujalowski,W. and Lohman,T.M. (1994) Co-operative binding of *Escherichia coli* SSB tetramers to single-stranded DNA in the (SSB)35 binding mode. *J. Mol. Biol.*, **236**, 106–123.
44. Oliveira,M.T. and Kaguni,L.S. (2011) Reduced stimulation of recombinant DNA polymerase gamma and mitochondrial DNA (mtDNA) helicase by variants of mitochondrial single-stranded DNA-binding protein (mtSSB) correlates with defects in mtDNA replication in animal cells. *J. Biol. Chem.*, **286**, 40649–40658.
45. Raghunathan,S., Ricard,C.S., Lohman,T.M. and Waksman,G. (1997) Crystal structure of the homo-tetrameric DNA binding domain of *Escherichia coli* single-stranded DNA-binding protein determined by multiwavelength x-ray diffraction on the selenomethionyl protein at 2.9-A resolution. *Proc. Natl Acad. Sci. USA*, **94**, 6652–6657.
46. Yang,C., Curth,U., Urbanke,C. and Kang,C. (1997) Crystal structure of human mitochondrial single-stranded DNA binding protein at 2.4 A resolution. *Nat. Struct. Biol.*, **4**, 153–157.
47. Savvides,S.N., Raghunathan,S., Futterer,K., Kozlov,A.G., Lohman,T.M. and Waksman,G. (2004) The C-terminal domain of full-length *E. coli* SSB is disordered even when bound to DNA. *Protein Sci.*, **13**, 1942–1947.
48. DiDonato,M., Krishna,S.S., Schwarzenbacher,R., McMullan,D., Jaroszewski,L., Miller,M.D., Abdubek,P., Agarwalla,S., Ambing,E., Axelrod,H. *et al.* (2006) Crystal structure of a single-stranded DNA-binding protein (TM0604) from *Thermotoga maritima* at 2.60 A resolution. *Proteins*, **63**, 256–260.
49. Shereda,R.D., Reiter,N.J., Butcher,S.E. and Keck,J.L. (2009) Identification of the SSB binding site on *E. coli* RecQ reveals a conserved surface for binding SSB's C terminus. *J. Mol. Biol.*, **386**, 612–625.
50. Oliveira,M.T. and Kaguni,L.S. (2010) Functional roles of the N- and C-terminal regions of the human mitochondrial single-stranded DNA-binding protein. *PLoS One*, **5**, e15379.
51. Curth,U., Urbanke,C., Greipel,J., Gerberding,H., Tiranti,V. and Zeviani,M. (1994) Single-stranded-DNA-binding proteins from human mitochondria and *Escherichia coli* have analogous physicochemical properties. *Eur. J. Biochem.*, **221**, 435–443.
52. Purnapatre,K. and Varshney,U. (1999) Cloning, over-expression and biochemical characterization of the single-stranded DNA binding protein from *Mycobacterium tuberculosis*. *Eur. J. Biochem.*, **264**, 591–598.
53. Opresko,P.L., Mason,P.A., Podell,E.R., Lei,M., Hickson,I.D., Cech,T.R. and Bohr,V.A. (2005) POT1 stimulates RecQ helicases WRN and BLM to unwind telomeric DNA substrates. *J. Biol. Chem.*, **280**, 32069–32080.
54. Rajagopal,V. and Patel,S.S. (2008) Single strand binding proteins increase the processivity of DNA unwinding by the hepatitis C virus helicase. *J. Mol. Biol.*, **376**, 69–79.
55. Bugreev,D.V., Mazina,O.M. and Mazin,A.V. (2009) Bloom syndrome helicase stimulates RAD51 DNA strand exchange activity through a novel mechanism. *J. Biol. Chem.*, **284**, 26349–26359.
56. Sowd,G., Wang,H., Pretto,D., Chazin,W.J. and Opresko,P.L. (2009) Replication protein A stimulates the Werner syndrome protein branch migration activity. *J. Biol. Chem.*, **284**, 34682–34691.
57. Alberts,B.M. and Frey,L. (1970) T4 bacteriophage gene 32: a structural protein in the replication and recombination of DNA. *Nature*, **227**, 1313–1318.
58. Gavin,A.C., Aloy,P., Grandi,P., Krause,R., Boesche,M., Marzioch,M., Rau,C., Jensen,L.J., Bastuck,S., Dumpelfeld,B. *et al.* (2006) Proteome survey reveals modularity of the yeast cell machinery. *Nature*, **440**, 631–636.
59. Tarassov,K., Messier,V., Landry,C.R., Radinovic,S., Serna Molina,M.M., Shames,I., Malitskaya,Y., Vogel,J., Bussey,H. and Michnick,S.W. (2008) An in vivo map of the yeast protein interactome. *Science*, **320**, 1465–1470.
60. Batisse,J., Batisse,C., Budd,A., Bottcher,B. and Hurt,E. (2009) Purification of nuclear poly(A)-binding protein Nab2 reveals association with the yeast transcriptome and a messenger ribonucleoprotein core structure. *J. Biol. Chem.*, **284**, 34911–34917.
61. Dekker,C., Stirling,P.C., McCormack,E.A., Filmore,H., Paul,A., Brost,R.L., Costanzo,M., Boone,C., Leroux,M.R. and Willison,K.R. (2008) The interaction network of the chaperonin CCT. *EMBO J.*, **27**, 1827–1839.
62. Akiyoshi,B., Sarangapani,K.K., Powers,A.F., Nelson,C.R., Reichow,S.L., Arellano-Santoyo,H., Gonen,T., Ranish,J.A., Asbury,C.L. and Biggins,S. (2010) Tension directly stabilizes reconstituted kinetochore-microtubule attachments. *Nature*, **468**, 576–579.
63. Smart,S.K., Mackintosh,S.G., Edmondson,R.D., Taverna,S.D. and Tackett,A.J. (2009) Mapping the local protein interactome of the NuA3 histone acetyltransferase. *Protein Sci.*, **18**, 1987–1997.
64. Kucejova,B. and Foury,F. (2003) Search for protein partners of mitochondrial single-stranded DNA-binding protein Rim1p using a yeast two-hybrid system. *Folia Microbiol. (Praha)*, **48**, 183–188.
65. Collins,S.R., Kemmeren,P., Zhao,X.C., Greenblatt,J.F., Spencer,F., Holstege,F.C., Weissman,J.S. and Krogan,N.J. (2007) Toward a comprehensive atlas of the physical interactome of *Saccharomyces cerevisiae*. *Mol. Cell Proteomics*, **6**, 439–450.
66. Breitkreutz,A., Choi,H., Sharom,J.R., Boucher,L., Neduva,V., Larsen,B., Lin,Z.Y., Breitkreutz,B.J., Stark,C., Liu,G. *et al.* (2010) A global protein kinase and phosphatase interaction network in yeast. *Science*, **328**, 1043–1046.
67. Vongsamphanh,R., Fortier,P.K. and Ramotar,D. (2001) Pir1p mediates translocation of the yeast Apn1p endonuclease into the mitochondria to maintain genomic stability. *Mol. Cell Biol.*, **21**, 1647–1655.
68. Symington,L.S. (2002) Role of RAD52 epistasis group genes in homologous recombination and double-strand break repair. *Microbiol. Mol. Biol. Rev.*, **66**, 630–670, table.
69. Meeusen,S., Tieu,Q., Wong,E., Weiss,E., Schieltz,D., Yates,J.R. and Nunnari,J. (1999) Mgm101p is a novel component of the mitochondrial nucleoid that binds DNA and is required for the repair of oxidatively damaged mitochondrial DNA. *J. Cell Biol.*, **145**, 291–304.
70. Bae,S.H. and Seo,Y.S. (2000) Characterization of the enzymatic properties of the yeast dna2 Helicase/endonuclease suggests a new model for Okazaki fragment processing. *J. Biol. Chem.*, **275**, 38022–38031.
71. Contamine,V. and Picard,M. (2000) Maintenance and integrity of the mitochondrial genome: a plethora of nuclear genes in the budding yeast. *Microbiol. Mol. Biol. Rev.*, **64**, 281–315.
72. O'Rourke,T.W., Doudican,N.A., Zhang,H., Eaton,J.S., Doetsch,P.W. and Shadel,G.S. (2005) Differential involvement of the related DNA helicases Pif1p and Rrm3p in mtDNA point mutagenesis and stability. *Gene*, **354**, 86–92.
73. Doudican,N.A., Song,B., Shadel,G.S. and Doetsch,P.W. (2005) Oxidative DNA damage causes mitochondrial genomic instability in *Saccharomyces cerevisiae*. *Mol. Cell Biol.*, **25**, 5196–5204.
74. Taylor,S.D., Zhang,H., Eaton,J.S., Rodeheffer,M.S., Lebedeva,M.A., O'Rourke,T.W., Siede,W. and Shadel,G.S. (2005) The conserved Mec1/Rad53 nuclear checkpoint pathway regulates

mitochondrial DNA copy number in *Saccharomyces cerevisiae*. *Mol. Biol. Cell*, **16**, 3010–3018.
75. Yu,E.Y., Wang,F., Lei,M. and Lue,N.F. (2008) A proposed OB-fold with a protein-interaction surface in *Candida albicans* telomerase protein Est3. *Nat. Struct. Mol. Biol.*, **15**, 985–989.
76. Xu,D., Guo,R., Sobeck,A., Bachrati,C.Z., Yang,J., Enomoto,T., Brown,G.W., Hoatlin,M.E., Hickson,I.D. and Wang,W. (2008) RMI, a new OB-fold complex essential for Bloom syndrome protein to maintain genome stability. *Genes Dev.*, **22**, 2843–2855.
77. Carpentieri,F., De,F.M., De,F.M., Rossi,M. and Pisani,F.M. (2002) Physical and functional interaction between the mini-chromosome maintenance-like DNA helicase and the single-stranded DNA binding protein from the crenarchaeon *Sulfolobus solfataricus*. *J. Biol. Chem.*, **277**, 12118–12127.
78. Marsh,V.L., McGeoch,A.T. and Bell,S.D. (2006) Influence of chromatin and single strand binding proteins on the activity of an archaeal MCM. *J. Mol. Biol.*, **357**, 1345–1350.
79. Kozlov,A.G., Jezewska,M.J., Bujalowski,W. and Lohman,T.M. (2010) Binding specificity of Escherichia coli single-stranded DNA binding protein for the chi subunit of DNA pol III holoenzyme and PriA helicase. *Biochemistry*, **49**, 3555–3566.
80. Bochkarev,A. and Bochkareva,E. (2004) From RPA to BRCA2: lessons from single-stranded DNA binding by the OB-fold. *Curr. Opin. Struct. Biol.*, **14**, 36–42.
81. Cheng,X. and Ivessa,A.S. (2010) Association of the yeast DNA helicase Pif1p with mitochondrial membranes and mitochondrial DNA. *Eur. J. Cell Biol.*, **89**, 742–747.
82. Diffley,J.F. and Stillman,B. (1991) A close relative of the nuclear, chromosomal high-mobility group protein HMG1 in yeast mitochondria. *Proc. Natl Acad. Sci. USA*, **88**, 7864–7868.
83. Sedman,T., Kuusk,S., Kivi,S. and Sedman,J. (2000) A DNA helicase required for maintenance of the functional mitochondrial genome in *Saccharomyces cerevisiae*. *Mol. Cell Biol.*, **20**, 1816–1824.
84. Sedman,T., Joers,P., Kuusk,S. and Sedman,J. (2005) Helicase Hmi1 stimulates the synthesis of concatemeric mitochondrial DNA molecules in yeast *Saccharomyces cerevisiae*. *Curr. Genet.*, **47**, 213–222.
85. Chattopadhyay,S., Chen,Y. and Weller,S.K. (2006) The two helicases of herpes simplex virus type 1 (HSV-1). *Front. Biosci.*, **11**, 2213–2223.
86. Bochman,M.L. and Schwacha,A. (2009) The Mcm complex: unwinding the mechanism of a replicative helicase. *Microbiol. Mol. Biol. Rev.*, **73**, 652–683.
87. George,T., Wen,Q., Griffiths,R., Ganesh,A., Meuth,M. and Sanders,C.M. (2009) Human Pif1 helicase unwinds synthetic DNA structures resembling stalled DNA replication forks. *Nucleic Acids Res.*, **37**, 6491–6502.
88. Piazza,A., Boule,J.B., Lopes,J., Mingo,K., Largy,E., Teulade-Fichou,M.P. and Nicolas,A. (2010) Genetic instability triggered by G-quadruplex interacting Phen-DC compounds in *Saccharomyces cerevisiae*. *Nucleic Acids Res.*, **38**, 4337–4348.
89. Paeschke,K., Capra,J.A. and Zakian,V.A. (2011) DNA replication through G-quadruplex motifs is promoted by the *Saccharomyces cerevisiae* Pif1 DNA helicase. *Cell*, **145**, 678–691.
90. Capra,J.A., Paeschke,K., Singh,M. and Zakian,V.A. (2010) G-quadruplex DNA sequences are evolutionarily conserved and associated with distinct genomic features in *Saccharomyces cerevisiae*. *PLoS Comput. Biol.*, **6**, e1000861.